Inorg. Chem. **2007**, *46*, 3752–3767

Ligand Topology Variations and the Importance of Ligand Field Strength in Non-Heme Iron Catalyzed Oxidations of Alkanes

Jason England, George J. P. Britovsek,* Nitin Rabadia, and Andrew J. P. White

Department of Chemistry, Imperial College London, Exhibition Road, London, SW7 2AY, United Kingdom

Received January 14, 2007

A series of iron(II)–bis(triflate) complexes $[Fe(L)(OTf)_2]$ containing linear tetradentate bis(quinolyl)-diamine and bis-(quinolylmethyl)-diamine ligands with a range of ligand backbones has been prepared. The coordination geometries of these complexes have been investigated in the solid state by X-ray crystallography and in solution by ^1H and ^{19}F NMR spectroscopy. Because of the labile nature of high-spin iron(II) complexes in solution, dynamic equilibria of complexes with different coordination geometries (cis-α, cis-β, and trans) are observed with certain ligand systems. In these cases, the geometry observed in the solid-state does not necessarily represent the only or even the major geometry present in solution. The ligand field strength in the various complexes has been investigated by variable-temperature (VT) magnetic moment measurements and by UV–vis spectroscopy. The strongest ligand field is observed with the most rigid ligand that generates $[Fe(L)(OTf)_2]$ complexes with a cis-α coordination geometry, and the corresponding $[Fe(L)(CH_3CN)_2]^{2+}$ complex displays spin crossover behavior. The catalytic properties of the complexes for the oxidation of cyclohexane have been investigated using hydrogen peroxide as the oxidant. An increased flexibility in the ligand results in a weaker ligand field, which increases the lability of the complexes. The activity and selectivity of the catalysts appear to be related to the strength of the ligand field and the stability of the catalyst.

Introduction

The combination of hydrogen peroxide and ferrous ions (Fenton's reagent) has long been known to produce species capable of oxidizing a wide variety of organic substrates, including hydrocarbons.[1] This reaction proceeds via an autoxidative mechanism, which involves freely diffusing alkyl radicals,[2−4] and in the presence of dioxygen, the primary product is usually an alkyl hydroperoxide.[3] Many attempts have been made to modify the reactivity and selectivity of the simple Fenton system by the addition of additives or by the coordination of ligands to the metal center, for example, the oxygenated Fenton system[5,6] or the Gif system,[7,8] but the autoxidative mechanism remains the dominant reaction pathway in the majority of cases.[9−12] However, during the past decade some important exceptions to this have emerged. Several non-heme iron catalysts have shown, in combination with hydrogen peroxide, a more atom-efficient oxidation reactivity, better conversions of H_2O_2 into product, less decomposition of H_2O_2, and a more selective oxidation reactivity, including stereospecific and dioxygen-independent hydroxylation of unactivated alkanes.[13−15] The observed C−H selectivities and kinetic isotope effects (KIE) are also indicative of a more selective oxidant than those that are responsible for oxidation in Fenton-type systems. Isotope labeling studies[16] and density functional theory (DFT)

* To whom correspondence should be addressed. E-mail: g.britovsek@imperial.ac.uk.

(1) Fenton, H. J. H. *J. Chem. Soc.* **1894**, *65*, 899−910.
(2) Walling, C. *Acc. Chem. Res.* **1975**, *8*, 125−131.
(3) Gozzo, F. *J. Mol. Catal.* **2001**, *171*, 1−22.
(4) Dunford, H. B. *Coord. Chem. Rev.* **2002**, *233*−*234*, 311−318.
(5) Sawyer, D. T. *Coord. Chem. Rev.* **1997**, *165*, 297−313.
(6) Sawyer, D. T.; Sobkowiak, A.; Matsushita, T. *Acc. Chem. Res.* **1996**, *29*, 409−416.
(7) Barton, D. H. R.; Doller, D. *Acc. Chem. Res.* **1992**, *25*, 504−512.
(8) Barton, D. H. R. *Chem. Soc. Rev.* **1996**, 237−239.
(9) Stavropoulos, P.; Çelenligil-Çetin, R.; Tapper, A. E. *Acc. Chem. Res.* **2001**, *34*, 745−752.
(10) Perkins, M. J. *Chem. Soc. Rev.* **1996**, 229−236.
(11) MacFaul, P. A.; Wayner, D. D. M.; Ingold, K. U. *Acc. Chem. Res.* **1998**, *31*, 159−162.
(12) Walling, C. *Acc. Chem. Res.* **1998**, *31*, 155−157.
(13) Chen, K.; Que Jr., L. *J. Am. Chem. Soc.* **2001**, *123*, 6327−6337.
(14) (a) Costas, M.; Chen, K.; Que, L., Jr. *Coord. Chem. Rev.* **2000**, *200*−*202*, 517−544. (b) Tanase, S.: Bouwman, E. *Adv. Inorg. Chem.* **2006**, *58*, 29−75.
(15) Kryatov, S. V.; Rybak-Akimova, E. V.; Schindler, S. *Chem. Rev.* **2005**, *105*, 2175−2226.
(16) Chen, K.; Costas, M.; Que, L., Jr. *Dalton Trans.* **2002**, 672−679.

10.1021/ic070062r CCC: $37.00
Published on Web 04/06/2007

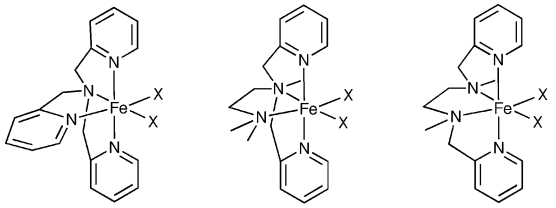

Figure 1. Examples of non-heme iron oxidation catalysts.

calculations[17] implicate an iron(V) oxo complex as the active oxidant,[16] which suggests that the reaction mechanism is analogous to that accepted for cytochrome P-450 systems[18] (i.e., hydrogen atom abstraction followed by a rapid oxygen rebound).[19]

Efficient non-heme iron(II) catalyst systems typically contain either tripodal tetradentate ligands such as TPA[20,21] and *iso*-BPMEN,[22] or linear tetradentate ligands such as BPMEN[23] (Figure 1). Common features in these systems are the use of multidentate ligands with at least two pyridine donors and labile co-ligands X (e.g., weakly coordinating triflate anions or acetonitrile molecules (CH_3CN) in combination with non-coordinating anions).

Iron(II) complexes containing the linear tetradentate pyridylmethylamine ligand BPMEN are currently the most efficient catalysts for the conversion of alkanes and hydrogen peroxide into oxygenated alkane products. One of the main questions that arises is why this particular complex exhibits higher atom efficiency than other non-heme iron(II) catalysts. Furthermore, other than the requirement for a pair of cis-labile sites, which is accommodated in BPMEN complexes due to the preferred cis-α coordination mode of the ligand, what other factors are significant in determining the catalytic properties of a complex? The cyclohexyl derivative BPMCN has been shown to give iron(II) complexes with either a cis-α or a cis-β geometry, depending on the synthesis route used, and their respective catalytic reactivities were found to be quite different.[24] We have shown recently that biphenyl-bridged analogues give rise to a trans geometry with a catalytic activity resembling Fenton-type reactivity.[25] So far, there appears to be a very limited understanding of the ligand-based requirements for the formation of an iron(II) complex capable of preferentially promoting the oxygen rebound mechanism.

As part of our alkane oxidation program, which aims to enhance the understanding of ligand-based requirements for the formation of efficient catalysts capable of the non-autoxidative oxidation of hydrocarbons using hydrogen peroxide as the oxidant, we have prepared a series of novel iron(II) complexes with ligands incorporating quinolyl or quinolylmethyl units as in BQEN (**1**), BQCN (**2**), $BQMe_2$-PN (**3**), BQPN (**4**), and BQMEN (**5**) (see Figure 2). The coordination geometries, solution behaviors, and electronic properties of the iron(II) complexes have been investigated, and the activity and selectivity of these complexes as catalysts for the oxidation of cyclohexane, using hydrogen peroxide as the oxidant, have been determined and compared with those of $[Fe(BPMEN)(OTf)_2]$.

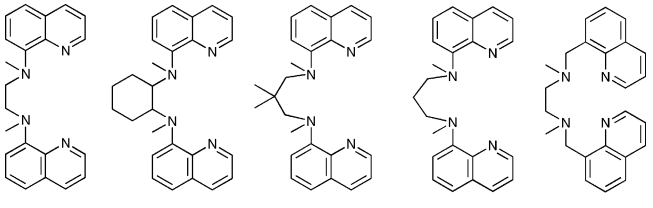

Figure 2. Quinoline-based ligand series **1**−**5**.

Results and Discussion

Ligand and Complex Synthesis. The quinoline-based ligands **1**−**3** were prepared via the generalized two-step procedure given in eq 1. The first step involves the preparation of the non-methylated secondary amines using a modified Bucherer reaction as previously reported by Nielsen and co-workers.[26] Modification of the workup procedure resulted in significantly better product yields. In the second step, deprotonation of the secondary amines using 2 equiv of *n*-butyl lithium resulted in the dianilide salts, which were subsequently reacted with methyl iodide to give the desired ligands **1**−**3**.

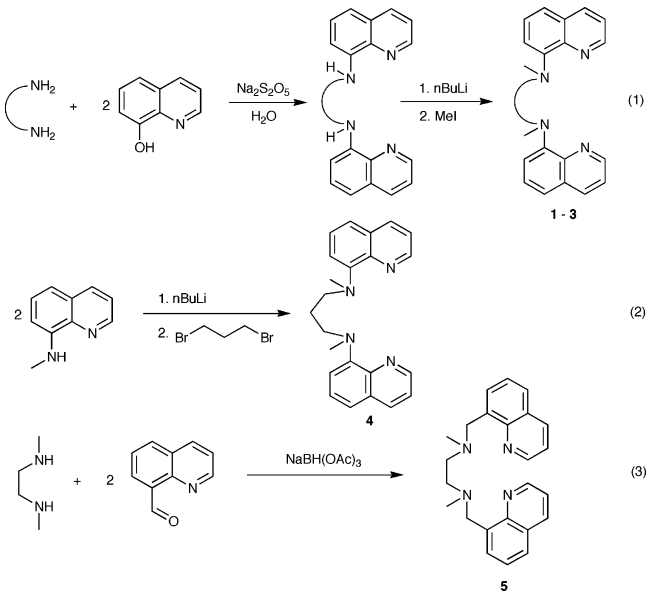

Attempts to prepare the propyl-bridged **4** via this procedure led to fragmentation at the methylation stage. It was found

(17) Bassan, A.; Blomberg, M. R. A.; Siegbahn, P. E. M.; Que, L., Jr. *Chem. −Eur. J.* **2005**, *11*, 692−705.
(18) Meunier, B.; de Visser, S. P.; Shaik, S. *Chem. Rev.* **2004**, *104*, 3947−3980.
(19) Groves, J. T. *J. Chem. Educ.* **1985**, *62*, 928−931.
(20) Kim, J.; Harrison, R. G.; Kim, C.; Que, L., Jr. *J. Am. Chem. Soc.* **1996**, *118*, 4373−4379.
(21) Lim, M. H.; Rohde, J.-U.; Stubna, A.; Bukowski, M. R.; Costas, M.; Ho, R. Y. N.; Münck, E.; Nam, W.; Que, L., Jr. *Proc. Natl. Acad. Sci. U.S.A.* **2003**, *100*, 3665−3670.
(22) Britovsek, G. J. P.; England, J.; White, A. J. P. *Inorg. Chem.* **2005**, *44*, 8125−8134.
(23) Chen, K.; Que, L., Jr. *Chem. Commun.* **1999**, 1375−1376.
(24) Costas, M.; Que, L., Jr. *Angew. Chem. Int. Ed.* **2002**, *41*, 2179−2181.
(25) Britovsek, G. J. P.; England, J.; White, A. J. P. *Dalton Trans.* **2006**, 1399−1408.
(26) Jensen, K. A.; Nielsen, P. H. *Acta Chem. Scand.* **1964**, *18*, 1−9.

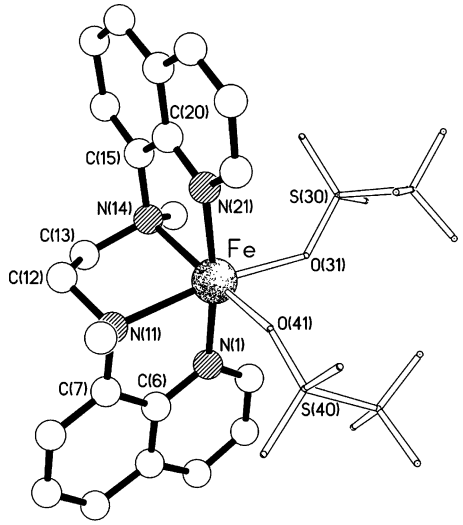

Figure 3. Molecular structure of [Fe(**1**)(OTf)$_2$].

Table 1. Selected Bond Lengths (Å) and Angles (°) for [Fe(**1**)(OTf)$_2$]

Fe−N(1)	2.1338(16)	Fe−N(11)	2.2677(16)
Fe−N(14)	2.2585(16)	Fe−N(21)	2.1438(16)
Fe−O(31)	2.1400(15)	Fe−O(41)	2.1039(15)
N(1)−Fe−O(41)	97.56(7)	N(1)−Fe−N(11)	77.74(6)
N(1)−Fe−N(14)	94.14(6)	N(1)−Fe−N(21)	170.92(6)
N(1)−Fe−O(31)	89.51(6)	N(11)−Fe−N(14)	81.42(6)
N(11)−Fe−N(21)	96.00(6)	N(11)−Fe−O(31)	167.17(6)
N(11)−Fe−O(41)	93.64(6)	N(14)−Fe−N(21)	78.30(6)
N(14)−Fe−O(31)	98.32(6)	N(14)−Fe−O(41)	166.06(6)
N(21)−Fe−O(31)	96.50(6)	N(21)−Fe−O(41)	89.33(7)
O(31)−Fe−O(41)	89.38(7)		

that this process could be suppressed by the substitution of the hydrogen atoms attached to the central methylene carbon atom with methyl groups, as in **3**. This implies that the decomposition proceeds via deprotonation at this carbon atom, a supposition that is supported by the observation of *N*,*N*-dimethyl-8-aminoquinoline as one of the main fragmentation products. Ligand **4** could, however, be prepared by the deprotonation of *N*-methyl-8-aminoquinoline with *n*-butyl lithium to give the corresponding anilide salt that is then reacted with 1,3-dibromopropane (eq 2). Ligand **5** was prepared by the reductive amination of 2 equiv of 8-formylquinoline with 1 equiv of *N*,*N*′-dimethylethylene-1,2-diamine (eq 3), with sodium triacetoxyborohydride as the reducing agent. Isolation and purification of the corresponding oxalate salt were performed, and the purified material was subsequently treated with aqueous base to release **5** as a pure material.

The iron(II) complexes [Fe(**1**)(OTf)$_2$], [Fe(**2**)(OTf)$_2$], [Fe(**3**)(OTf)$_2$], [Fe(**4**)(OTf)$_2$], and [Fe(**5**)(OTf)$_2$] were prepared by mixing tetrahydrofuran (THF) solutions of equimolar quantities of the ligands and Fe(OTf)$_2$(CH$_3$CN)$_2$ at room temperature (RT). The solid-state and solution properties of these complexes were analyzed by X-ray analysis, multinuclear NMR and UV−vis spectroscopy, and magnetic susceptibility measurements.

Triflate anions are highly labile ligands that are easily displaced by other coordinating ligands. For example, in acetonitrile [Fe(BPMEN)(OTf)$_2$] forms the dicationic solvento complex [Fe(BPMEN)(CH$_3$CN)$_n$]$^{2+}$.[22] Although the triflate anions readily behave as counterions, they can be coordinating, and in the case of the aforementioned solvento complex there was evidence of a rapid equilibrium with triflate coordinated species. To further examine the competitive coordination between the weakly coordinating triflate anions and the acetonitrile molecules, an analogue of the [Fe(**1**)(OTf)$_2$] complex was prepared with perchlorate anions to form [Fe(**1**)(CH$_3$CN)$_2$](ClO$_4$)$_2$. The perchlorate anions are very weakly coordinating and in the presence of acetonitrile they would be expected to behave solely as counteranions. This complex was prepared by dissolving equimolar quantities of iron(II) perchlorate hydrate and **1** in acetonitrile. Subsequent to stirring the mixture for several hours, the product was isolated as a red-brown solid and purified by recrystallization from an acetonitrile solution with diethyl ether.

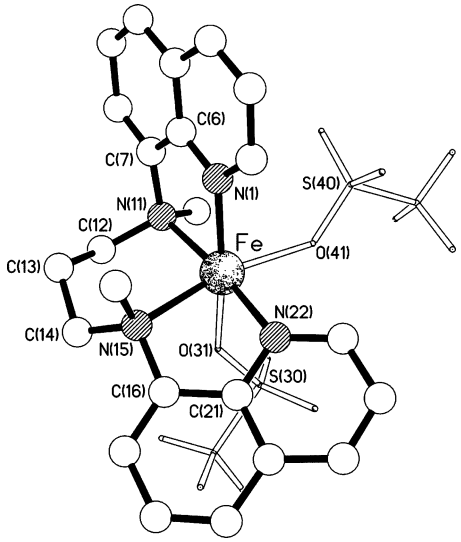

Figure 4. Molecular structure of one (**I**) of the two crystallographically independent molecules present in the crystals of [Fe(**4**)(OTf)$_2$].

Solid-State Structures. The X-ray analysis of crystals of the [Fe(**1**)(OTf)$_2$] complex showed the ligand had adopted a cis-α coordination mode around the distorted octahedral metal center (Figure 3 and Table 1). The Fe bond distances are typical for high spin (HS) iron(II) complexes, and they are similar to those seen in the related HS complexes [Fe(BPMEN)Cl$_2$] and [Fe(5-Me$_2$−BPMEN)(OTf)$_2$].[27,28] The Fe bond distances of the trans quinoline nitrogens [Fe−N(1) = 2.1338(16) and Fe−N(21) = 2.1438(16) Å] are noticeably shorter than those of the amine nitrogens N(11) and N(14) [2.2677(16) and 2.2585(16) Å, respectively]. The absolute configuration of the amine nitrogen atoms in the stereoisomer shown in Figure 3 is (*S*,*S*).

The X-ray structure of the [Fe(**4**)(OTf)$_2$] complex revealed the presence of two crystallographically independent molecules (**I** and **II**) in the asymmetric unit; molecule **I** is shown in Figure 4, and molecule **II** is shown in Figure S2 (Supporting Information). Except for the orientation of the

(27) Chen, K.; Costas, M.; Kim, J.; Tipton, A.; Que, L., Jr. *J. Am. Chem. Soc.* **2002**, *124*, 3026−3035.
(28) Raffard, N.; Balland, V.; Simaan, A. J.; Létard, S.; Nierlich, M.; Miki, K.; Banse, F.; Anxolabéhère-Mallart, E.; Girerd, J.-J. *C. R. Chim.* **2002**, *5*, 99−109.

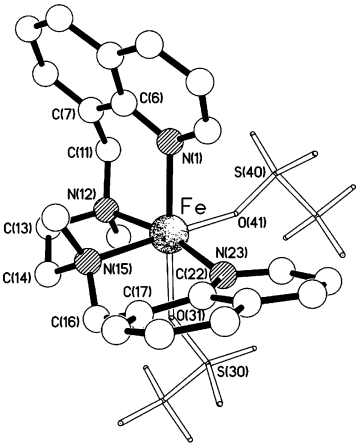

Figure 5. Molecular structure of [Fe(**5**)(OTf)$_2$].

S(40) triflate ligand, the two molecules have essentially the same geometry, with the root-mean-square (rms) fit of all of the non-hydrogen atoms of the two complexes (excluding the non-coordinated O_2SCF_3 atoms of the S(40) triflate moiety) being ca. 0.098 Å (Figure S5, Supporting Information). In each case the ligand has adopted a cis-β coordination mode around a distorted octahedral metal center. The Fe−N(quin) bond lengths are significantly shorter than the Fe−N(amine) bond lengths, but they are comparable overall to a similar complex with a cis-β geometry, [Fe(5-Me$_2$−BPMCN)(OTf)$_2$].[29] Interestingly, the two five-membered chelate rings in [Fe(**4**)(OTf)$_2$] have very different conformations; whereas the N(1)/N(11) ring is essentially flat (coplanar to within ca. 0.02 Å [0.03 Å]), the N(15)/N(22) has a very marked envelope conformation, with the metal lying ca. 0.88 Å [0.92 Å] out of the C_2N_2 plane (the values for molecule **II** are given in square parentheses). The six-membered chelate ring has a chair conformation with Fe and C(13) lying ca. +0.68 and −0.75 Å [+0.69 and −0.75 Å] out of the {N(11),C(12),C(14),N(15)} plane, which is coplanar to within ca. 0.01 Å [0.02 Å]. The absolute configuration of the amine nitrogen atoms in the stereoisomer shown in Figure 4 is (*S*,*S*).

The solid-state structure of [Fe(**5**)(OTf)$_2$] revealed the tetradentate **5** to have adopted a cis-β coordination mode around a distorted octahedral iron center (Figure 5), but with two partial occupancy orientations of the N(15) to N(23) portion (Figure S7, Supporting Information). This apparent "disorder" actually represents the superimposition of two distinct diastereomeric complexes in a ca. 75:25 ratio; the major (*S*,*S*) diastereoisomer is shown in Figure 5, and the minor (*S*,*R*) isomer involves an inversion of the stereochemistry of the N(15) center (the crystallographic space group is centrosymmetric, so for each diastereoisomer the enantiomer is also present). The following discussion will concentrate on the major diastereoisomer with the cis-β (*S*,*S*) configuration. The Fe−N bond lengths are significantly longer compared to the previous [Fe(**4**)(OTf)$_2$] complex, with the Fe−N(quin) bond trans to triflate [Fe−N(1) = 2.230(2) Å] being longer than that trans to nitrogen [Fe−N(23) = 2.215(3) Å] (Table 3). The six-membered chelate rings adopt an asymmetric boat conformation. The five-membered N(12)/N(15) chelate ring has an envelope conformation with C(14) positioned ca. 0.64 Å out of the {Fe,N(12),C(13),N(15)} plane, which is coplanar to within ca. 0.03 Å.

From these structural investigations we can conclude that complex [Fe(**1**)(OTf)$_2$] appears to prefer the cis-α coordination geometry in the solid-state, whereas complexes [Fe(**4**)(OTf)$_2$] and [Fe(**5**)(OTf)$_2$] prefer the cis-β geometry. Considering the small difference, the dimethyl analogue [Fe(**3**)(OTf)$_2$] is likely to show a similar preference for the cis-β geometry as in [Fe(**4**)(OTf)$_2$]. The solid-state geometry of the cyclohexyl derivative [Fe(**2**)(OTf)$_2$] is less predictable as both cis-α and cis-β geometries have been observed in the case of the analogous complex [Fe(BPMCN)(OTf)$_2$].[24,25]

Magnetic Susceptibility Measurements. The magnetic moments of the iron(II) bis(triflate) complexes containing ligands **1**−**5**, which were measured in CD_3CN and CD_2Cl_2 solution at 298 K using Evans' NMR method, are listed in Table 4. As expected from the weak ligand field exerted by the triflate anions, CD_2Cl_2 solutions of all complexes display magnetic moments consistent with HS iron(II) ($S = 2$) centers. In a CD_3CN solution, the triflate anions would be expected to be displaced by the stronger field acetonitrile ligands to yield dicationic complexes of the form [Fe(L)(CH$_3$CN)$_n$]$^{2+}$. In the case of [Fe(**2**)(OTf)$_2$], [Fe(**3**)(OTf)$_2$], [Fe(**4**)(OTf)$_2$], and [Fe(**5**)(OTf)$_2$], the μ_{eff} values are consistent with their formulation as HS iron(II) complexes at RT. In contrast, the μ_{eff} value measured for [Fe(**1**)(OTf)$_2$] at 298 K in CD_3CN was found to be intermediate between that expected for a HS and a low spin (LS) iron(II) center, which is suggestive of spin crossover (SC) behavior .[30,31]

The magnetic behavior of these iron(II) complexes in a CD_3CN solution was further investigated by measurement of their magnetic moments over the temperature range 233−343 K, using Evans' NMR method (Figure 6). The magnetic moment of complex [Fe(**3**)(OTf)$_2$] (and also of [Fe(**4**)(OTf)$_2$] and of [Fe(**5**)(OTf)$_2$], although not shown for clarity) remains fully HS upon cooling. The magnetic moment of the cyclohexyl derivative [Fe(**2**)(OTf)$_2$] decreases to $\mu_{eff} = 4.0\ \mu_B$ at 233 K and [Fe(**1**)(OTf)$_2$] undergoes a full spin transition within the temperature range. For comparison, we have also measured [Fe(BPMEN)(OTf)$_2$], which shows a similar magnetic behavior as [Fe(**1**)(OTf)$_2$] and the previously reported complex [Fe(BPMEN)(CH$_3$CN)$_2$](ClO$_4$)$_2$.[32] Collectively, the magnetic moments show that the quinolyl ligands that exclusively form five-membered chelate rings upon coordination (**1** and **2**) exert a stronger ligand field than those that incorporate six-membered chelate rings (**3**−**5**).

The thermodynamic parameters (ΔH°_{SC} and ΔS°_{SC}) associated with the SC process for [Fe(**1**)(OTf)$_2$] and [Fe(**1**)(CH$_3$CN)$_2$](ClO$_4$)$_2$ in a CD_3CN solution have been deter-

(29) Costas, M.; Rohde, J.-U.; Stubna, A.; Ho, R. Y. N.; Quaroni, L.; Münck, E.; Que, L., Jr. *J. Am. Chem. Soc.* **2001**, *123*, 12931−12932.
(30) Gütlich, P.; Garcia, Y.; Goodwin, H. A. *Chem. Soc. Rev.* **2000**, *29*, 419−427.
(31) Toftlund, H.; McGarvey, J. J. *Top. Curr. Chem.* **2004**, *233*, 151−166.
(32) Bryliakov, K. P.; Duban, E. A.; Talsi, E. P. *Eur. J. Inorg. Chem.* **2005**, 72−76.

Table 2. Selected Bond Lengths (Å) and Angles (°) for the Two Independent Molecules (**I** and **II**) Present in the Crystals of [Fe(**4**)(OTf)$_2$]

	Mol **I**	Mol **II**		Mol **I**	Mol **II**
Fe−N(1)	2.1297(16)	2.1208(16)	Fe−N(11)	2.2166(14)	2.2282(15)
Fe−N(15)	2.2572(15)	2.2773(16)	Fe−N(22)	2.1567(16)	2.1640(16)
Fe−O(31)	2.1466(14)	2.1197(14)	Fe−O(41)	2.1671(13)	2.1861(14)
N(1)−Fe−N(11)	79.27(6)	78.98(6)	N(1)−Fe−N(15)	97.24(6)	97.79(6)
N(1)−Fe−N(22)	101.77(6)	100.64(6)	N(1)−Fe−O(31)	167.38(6)	167.41(6)
N(1)−Fe−O(41)	89.45(6)	87.98(6)	N(11)−Fe−N(15)	97.19(5)	95.48(6)
N(11)−Fe−N(22)	173.56(6)	171.12(6)	N(11)−Fe−O(31)	88.40(5)	89.32(6)
N(11)−Fe−O(41)	95.52(5)	99.15(6)	N(15)−Fe−N(22)	76.38(6)	75.74(7)
N(15)−Fe−O(31)	86.87(6)	87.87(6)	N(15)−Fe−O(41)	166.54(6)	165.06(6)
N(22)−Fe−O(31)	90.78(6)	91.63(6)	N(22)−Fe−O(41)	90.86(6)	89.69(6)
O(31)−Fe−O(41)	89.08(5)	89.31(5)			

Table 3. Selected Bond Lengths (Å) and Angles (°) for [Fe(**5**)(OTf)$_2$]

Fe−N(1)	2.230(2)	Fe−N(12)	2.210(2)
Fe−N(15)	2.221(4)	Fe−N(23)	2.215(3)
Fe−O(31)	2.188(2)	Fe−O(41)	2.107(2)
N(1)−Fe−N(12)	89.20(9)	N(1)−Fe−N(15)	96.01(13)
N(1)−Fe−N(23)	98.00(16)	N(1)−Fe−O(31)	174.37(9)
N(1)−Fe−O(41)	88.91(9)	N(12)−Fe−N(15)	81.59(16)
N(12)−Fe−N(23)	167.71(18)	N(12)−Fe−O(31)	88.26(9)
N(12)−Fe−O(41)	91.97(10)	N(15)−Fe−N(23)	87.7(2)
N(15)−Fe−O(31)	88.59(13)	N(15)−Fe−O(41)	171.81(15)
N(23)−Fe−O(31)	85.41(16)	N(23)−Fe−O(41)	98.09(17)
O(31)−Fe−O(41)	86.16(9)		

mined by two methods: (1) from VT Evans' NMR data and (2) from the VT ^{1}H NMR chemical shifts. In the first method, the limiting HS and LS magnetic moments (μ_{HS} and μ_{LS}) are used to calculate the equilibrium constant K_{obs}, which provides ΔH°_{SC} and ΔS°_{SC}, according to the procedure described by Swanson and Crawford (Table 5).[33] The second method uses the chemical shift to determine K_{obs} (see Supporting Information for more details).[32]

The enthalpy and entropy changes associated with a purely thermally induced SC are generally on the order of $\Delta H^\circ_{SC} = 6-25$ kJ·mol^{-1} and $\Delta S^\circ_{SC} = 50-80$ J·K^{-1}·mol^{-1},[30,34−37] as observed for the complex $[Fe(tacn)_2]^{2+}$. The thermodynamic parameters determined for the iron(II) complexes containing the tetradentate ligands BPMEN and **1** are all significantly larger. In the case of [Fe(BPMEN)(CH$_3$CN)$_2$](ClO$_4$)$_2$, this has been attributed by Bryliakov and co-workers to the overlap between SC and an additional chemical process, such as the rapid dissociation/coordination of bound acetonitrile molecules at elevated temperature that gives rise to an equilibrium between six- and five-coordinate complexes.[32] It is most likely that such a process also occurs for the other SC complexes studied here and that this exchange process is affected by the nature of the anion, which gives rise to the small observed differences. The occurrence of such an exchange process/equilibrium is consistent with our previously reported NMR data on iron(II) bis(triflate) complexes of tripodal tetradentate nitrogen-donor ligands[22] and also with the studies of SC phenomena by Hagen and co-workers on iron(II) TPA complexes.[38]

(33) Crawford, T. H.; Swanson, J. *J. Chem. Educ.* **1971**, *48*, 382−386.
(34) Turner, J. W.; Schultz, F. A. *Inorg. Chem.* **2001**, *40*, 5296−5298.
(35) Al-Obaidi, A. H. R.; Jensen, K. B.; McGarvey, J. J.; Toftlund, H.; Jensen, B.; Bell, S. E. J.; Carroll, J. G. *Inorg. Chem.* **1996**, *35*, 5055−5060.
(36) König, E. *Struct. Bond.* **1991**, *76*, 51−152.
(37) Turner, J. W.; Schultz, F. A. *Inorg. Chem.* **1999**, *38*, 358−364.
(38) Diebold, A.; Hagen, K. S. *Inorg. Chem.* **1998**, *37*, 215−223.

^{1}H NMR Spectroscopy. The chemical shift range in the ^{1}H NMR spectra of HS Fe(II) complexes typically covers a shift range of about 200 ppm. In the case of complex [Fe(**1**)(OTf)$_2$], the spectrum measured in a CD$_3$CN solution at 298 K displays a relatively small chemical shift range of 0−50 ppm (Figure 7), which is consistent with the observed reduced magnetic moment of 3.72 μ_B. The assignment of the ^{1}H NMR spectrum was not straightforward due to severe line-broadening, as was seen in the spectrum of [Fe(BPMEN)(OTf)$_2$], which also exists in the SC domain in a CD$_3$CN solution at 298 K.[22] This line-broadening is attributed to the slow exchange of the acetonitrile ligands with the triflate counterions. Indeed, the ^{1}H NMR spectrum of the triflate-free analogue [Fe(**1**)(CH$_3$CN)$_2$](ClO$_4$)$_2$, which contains the more weakly coordinating ClO$_4^-$ anions, was found to have a similar chemical shift range but greatly reduced line-widths (Figure S8, Supporting Information).

Unambiguous peak assignment was achieved by measuring the ^{1}H NMR spectrum of a CD$_3$CN solution of complex [Fe(**1**)(CH$_3$CN)$_2$](ClO$_4$)$_2$ at regular temperature intervals over the liquid range of the solvent (see Figure S8, Supporting Information). At the lower temperature limit (233 K), the diamagnetic spectrum was assigned with the aid of correlation spectroscopy (COSY) NMR (Figures 8 and S9, Supporting Information). This spectrum was related to the RT spectrum by plotting the chemical shift of the individual resonances vs temperature (Figure 9). As expected from the SC behavior of this complex, the change in the chemical shifts was found to be consistent with non-Curie behavior. Line-broadening corresponding to a fluxional process was not observed over the temperature range studied. Additionally, at all temperatures the ^{1}H NMR spectra displayed nine resonances, which is consistent with time-averaged C_2 symmetry and retention of the cis-α geometry observed in the solid-state.

Each magnetically unique proton environment in [Fe(**1**)(CH$_3$CN)$_2$](ClO$_4$)$_2$ produced a single resonance across the full temperature range studied, which indicates that the equilibrium between the HS and LS configurations is significantly faster than the time scale of the NMR experiment. Under such conditions, the magnitude of the observed chemicals shifts (δ_{obs}) is dependent upon the bulk magnetic moment, and as a consequence it can be used to estimate the thermodynamic parameters associated with SC (see Supporting Information and Table 5).[32] The values obtained for complex [Fe(**1**)(CH$_3$CN)$_2$](ClO$_4$)$_2$, $\Delta H^\circ_{SC} = 33.3(3.4)$

Table 4. Selected Physical Data for Complexes [Fe(**1**)(OTf)$_2$]−[Fe(**5**)(OTf)$_2$]

	^{19}F in CD_2Cl_2[a]		^{19}F in CD_3CN[a]					
complex	δ (ppm)	$\nu_{1/2}$ (Hz)	δ (ppm)	$\nu_{1/2}$ (Hz)	λ_{max}[b] (nm)	ϵ_{max}[b] ($M^{-1}\cdot cm^{-1}$)	μ_{eff}[c] CD_2Cl_2 (BM)	μ_{eff}[c] CD_3CN (BM)
[Fe(**1**)(OTf)$_2$]	−25	820	−78.1	720	456	3600	5.4	3.7
[Fe(**2**)(OTf)$_2$]	−5	2300	−76.6	2970	447	940	4.9	5.4
	−17	200			402	930		
[Fe(**3**)(OTf)$_2$]	−17	1500	−68.1	2640	446	500	5.2	5.5
					387	800		
[Fe(**4**)(OTf)$_2$]	−5	1500	−69.7	1570	444	440	4.9	5.0
	−17	3000			382	750		
[Fe(**5**)(OTf)$_2$]	−20	1500	−69.8	715	365	750	4.9	5.1

[a] Measured at 298 K. [b] c = 0.5 mM in CH_3CN at 298 K. [c] Evans' NMR method at 298 K.

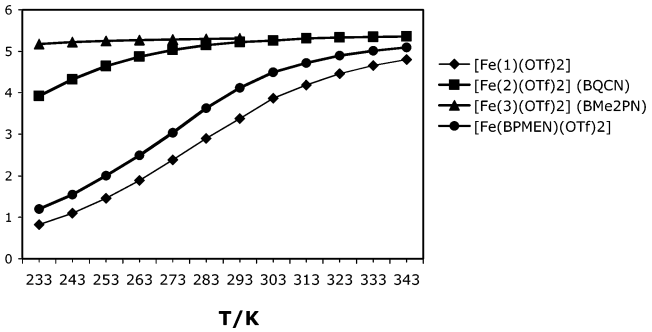

Figure 6. Magnetic moments (μ_{eff}) of selected iron(II) complexes in a CD_3CN solution as a function of temperature (T).

Table 5. Thermodynamic Parameters for the Spin-Crossover Process of Selected Iron Complexes[a]

complex	μ_{LS} (BM)	μ_{HS} (BM)	$T_{1/2}$ (K)	$\Delta H°_{SC}$ (kJ·mol^{-1})	$\Delta S°_{SC}$ (JK^{-1}·mol^{-1})	ref
VT Evans' NMR method						
[Fe(**1**)(OTf)$_2$]	0.46	5.18	299	35.1	117	
[Fe(**1**)(CH_3CN)$_2$](ClO_4)$_2$	1.48	4.95	311	33.5	107	
[Fe(BPMEN)(OTf)$_2$]	0.86	5.28	286	37.1	130	
[Fe(BPMEN)(CH_3CN)$_2$](ClO_4)$_2$	1.30	5.45	284	39.7(2.0)	135(9)	32
[Fe(tacn)$_2$]$^{2+}$ [b]	1.3	5.8	318	21(2)	66(6)	34
VT ^{1}H NMR						
[Fe(**1**)(OTf)$_2$]			311	36.7(1.3)	118.2(2.4)	
[Fe(**1**)(CH_3CN)$_2$](ClO_4)$_2$			313	33.3(3.4)	106.3(11.9)	
[Fe(BPMEN)(CH_3CN)$_2$](ClO_4)$_2$				40(3)	137(10)	32

[a] Measured in CD_3CN solution. [b] tacn = 1,4,7-triazacyclononane.

kJ·mol^{-1} and $\Delta S°_{SC}$ = 106.3(11.9) J·K^{-1}·mol^{-1}, are of similar magnitude to those obtained from VT Evans' NMR measurements and also are comparable to those determined by Bryliakov and co-workers for [Fe(BPMEN)(CH_3CN)$_2$](ClO_4)$_2$ ($\Delta H°_{SC}$ = 40(3) kJ·mol^{-1} and $\Delta S°_{SC}$ = 137(10) J·K^{-1}·mol^{-1}) under similar conditions.[32] These results reinforce the conclusions made previously on the basis of the magnetic susceptibility data, regarding the overlap between SC and additional chemical processes.

The thermodynamic parameters associated with SC were also determined for [Fe(**1**)(CH_3CN)$_2$](OTf)$_2$ (see Table 5). In this case, not all proton signals could be used due the line-broadening effect caused by triflate anion coordination. Variable temperature studies did, however, demonstrate that line-broadening began with the onset of SC and became increasingly severe with increasing temperature. The result was that, at 298 K, many resonances were not well resolved (see Figures 7 and S10, Supporting Information). However,

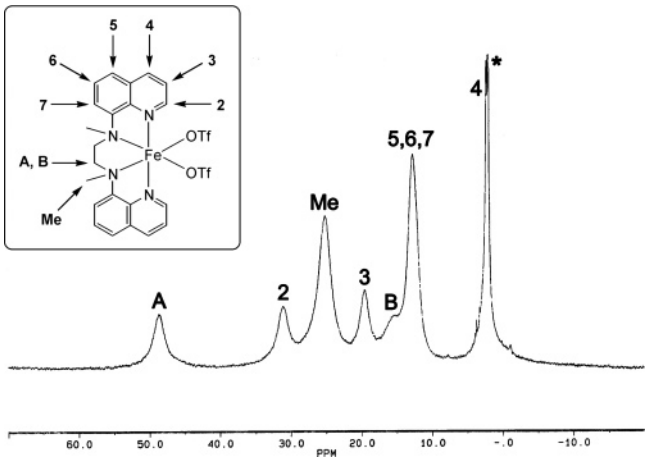

Figure 7. ^{1}H NMR spectrum of [Fe(**1**)(OTf)$_2$] in CD_3CN (*) solution at 298 K.

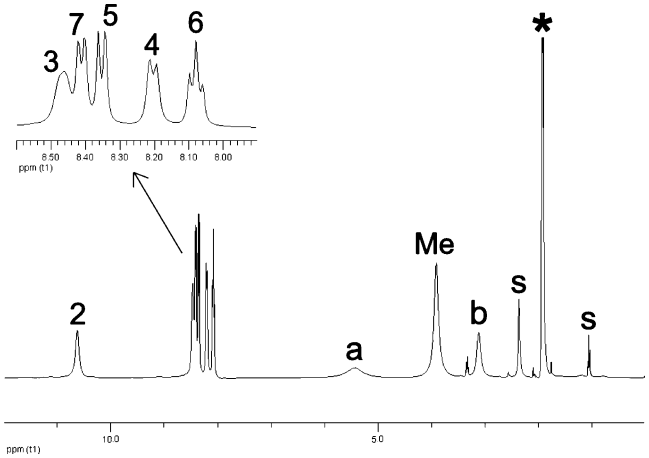

Figure 8. ^{1}H NMR spectrum of [Fe(1)(CH_3CN)$_2$](ClO_4)$_2$ in CD_3CN (*) solution at 233 K (for labeling see Figure 7; the label "s" indicates solvent residues).

at higher temperatures at which there is almost complete occupation of the HS configuration, the resonances were observed to sharpen and to give a well-resolved ^{1}H NMR spectrum, which is typical of a HS iron(II) complex (see Figure S10, Supporting Information). This line-broadening phenomenon is consistent with a fluxional process whose onset is commensurate with initiation of SC and becomes increasingly fast with increasing temperature. Similarly, the severe line-broadening observed in the ^{1}H NMR spectrum of the SC complex [Fe(BPMEN)(CH_3CN)$_2$](OTf)$_2$ in a CD_3CN solution at 298 K was found to disappear at higher

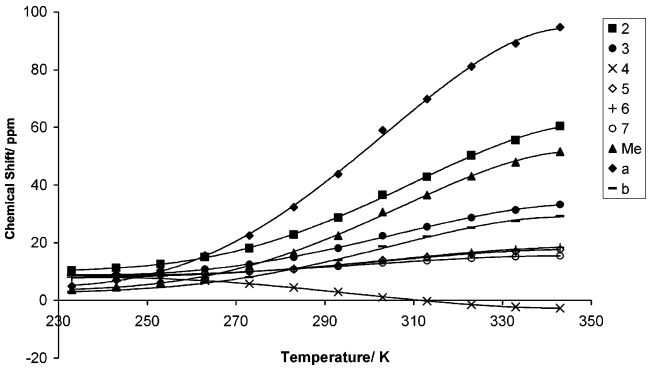

Figure 9. Variation of the ^{1}H NMR chemical shifts vs the temperature of [Fe(**1**)$(CH_3CN)_2$]$(ClO_4)_2$ in CD_3CN (for labeling see Figure 7).

temperatures, at which there is almost complete occupation of the HS configuration.

Although the thermally induced, commensurate onset of SC and of a fluxional process involving the triflate anions and acetonitrile ligands in complexes [Fe(BPMEN)$(OTf)_2$] and [Fe(**1**)$(OTf)_2$] could be coincidental, it is much more likely that they are related. The LS configuration appears to be accessible only for the dicationic bis(acetonitrile) species $[Fe(L)(CH_3CN)_2]^{2+}$, whereas triflate ligands and five-coordinate geometries do not exert a sufficiently strong ligand field to induce anything other than HS configurations in the temperature range accessible in liquid acetonitrile. HS-d^6 complexes are inherently more labile than LS-d^6 complexes and are therefore expected to readily dissociate an acetonitrile ligand and exchange with a triflate anion. The LS iron(II) complexes are generally much more substitutionally inert. Upon thermal initiation of SC, population of the HS configuration of $[Fe(L)(CH_3CN)_2]^{2+}$ would be observed from which a reduced energetic barrier to the formation of HS triflate-coordinated complexes, via an intermediary HS five-coordinate species, can be expected. These considerations represent a mechanism for the fluxional exchange of acetonitrile and triflate ligands initiated by SC (Scheme 1), which is consistent with the conclusions drawn from the thermodynamic parameters determined for the SC process.

In contrast to the ^{1}H NMR spectrum of [Fe(**1**)$(OTf)_2$] recorded in a CD_3CN solution, the spectrum recorded in a CD_2Cl_2 solution at 298 K is consistent with that expected for a HS iron(II) complex, i.e., relatively sharp peaks that exhibit strong contact shifts. The spectrum was assigned by comparison to the high-temperature (343 K) spectrum in CD_3CN, with assistance from the chemical shift magnitude and relative line-widths of the resonances.[39] Only seven resonances are observed, which indicates that two are absent. It is presumed that the absent signals correspond to the ethylene unit (a and b in Figure 8), because of the severe line-broadening that would result from their close proximity to the metal center. The high symmetry of the spectrum is consistent with a time-averaged C_2 symmetric cis-α geometry in a CD_2Cl_2 solution.

The ^{1}H NMR spectra of the HS complexes [Fe(**3**)$(OTf)_2$], [Fe(**4**)$(OTf)_2$], and [Fe(**5**)$(OTf)_2$] were assigned by using peak integration and by comparison with the spectra of [Fe(**1**)$(OTf)_2$]. Additional assistance was provided in some cases by the CD_3CN solution COSY spectrum (see, for example, Figure S11 for complex [Fe(**5**)$(OTf)_2$], Supporting Information). The most salient feature of the ^{1}H NMR spectra of these complexes is that they are all highly symmetrical in solution. In contrast to the cis-β geometry with C_1 symmetry, as observed in the solid-state structures of complexes [Fe(**4**)$(OTf)_2$] and [Fe(**5**)$(OTf)_2$], the solution structures appear to have time-averaged C_2 or C_s symmetry, which could be either the cis-α or trans geometry, with the latter seeming to be the most probable. The solid-state structure of the pyridylmethyl analogue of complex [Fe(**4**)$(OTf)_2$] (i.e., the propyl-bridged analogue of [Fe(BPMEN)$(OTf)_2$], see Figure 1), complex [Fe(BPMPN)$(OTf)_2$], was recently shown to have a C_s symmetric trans geometry in the solid-state.[40] A further notable facet of the ^{1}H NMR spectra of these three complexes is that there are insufficient peaks to fully account for all of those expected for a C_2 or C_s symmetric geometry. This suggests that the complexes are highly fluxional in solution and/or that a number of protons in each complex are sufficiently close to the iron(II) center that relaxation occurs faster than the time scale of the experiment.

The ^{1}H NMR spectrum of complex [Fe(**2**)$(OTf)_2$] measured in a CD_3CN solution at 298 K contains at least 18 resonances, which is many more than the 12 resonances expected for a cis-α configuration (Figure S12, Supporting information). There are two broad peaks at 92.1 and 72.0 ppm, which are assigned to two inequivalent N−Me groups. The possibility of diastereomer formation exists for this complex due to the chiral *trans*-1,2-cyclohexyldiamine backbone, but the ^{1}H NMR spectrum of the complex seems to be more consistent with a cis-β geometry. Depending on the method of preparation, iron(II) bis(triflate) complexes with either cis-α or cis-β geometry have been prepared for the related bis(pyridylmethyl)cyclohexyl analogue BPMCN.[24]

In addition to the equilibrium between five- and six-coordinate species, we can conclude from these ^{1}H NMR studies that for complexes [Fe(**4**)$(OTf)_2$] and [Fe(**5**)$(OTf)_2$] (and likely also [Fe(**3**)$(OTf)_2$]) the cis-β geometry seen in the solid-state is not retained in solution where a time-averaged C_2 or C_s symmetric geometry is observed, most likely the trans geometry. Complex [Fe(**2**)$(OTf)_2$] displays the C_1 symmetric cis-β geometry in solution, whereas complex [Fe(**1**)$(OTf)_2$] has the cis-α geometry both in the solid-state and in solution.

^{19}F NMR Spectroscopy. The dynamic behavior of the iron(II) triflate complexes was also studied by ^{19}F NMR spectroscopy. The chemical shift of the fluorine atoms in triflate anions, when bonded to diamagnetic centers or existing as non-coordinated anions, tends to be fairly independent of the chemical environment. For example, in

(39) Vedder, C.; Schaper, F.; Brintzinger, H. H.; Kettunen, M.; Babik, S.; Fink, G. *Eur. J. Inorg. Chem.* **2005**, 1071−1080.

(40) Mas-Ballesté, R.; Costas, M.; van den Berg, T.; Que, L., Jr. *Chem.—Eur. J.* **2006**, *12*, 7498−7500.

Scheme 1

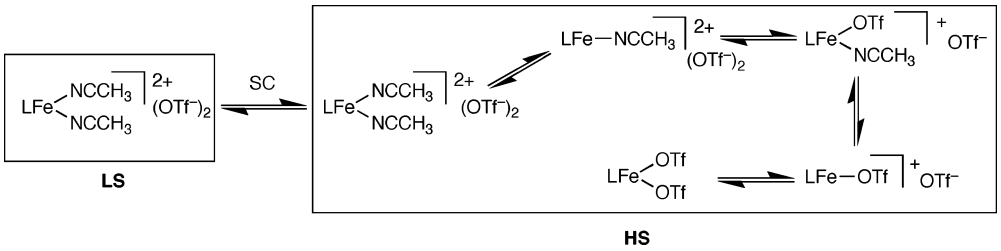

a CD_2Cl_2 solution at RT, the ^{19}F NMR spectrum of the covalently bound triflate in Me_3SiOTf exhibits a single peak at −78.7 ppm,[41] and the ionic triflate in [PPN]OTf (where PPN = $Ph_3P{=}N{=}PPh_3$) has a single resonance at −80.5 ppm.[42] Similarly, the ^{19}F resonance of triflate anions that are bound to diamagnetic transition metals are found in the region of −77 to −79 ppm.[43] In contrast, coordination to a paramagnetic center causes a significant contact shift. Consequently, the ^{19}F NMR spectrum of a HS iron(II) triflate complex at RT is strongly diagnostic as to whether the triflate anions are behaving as bridging ligands (ca. +60 ppm), as terminal ligands (ca. −10 ppm), or as counterions (ca. −80 ppm).[44,45]

In a CD_2Cl_2 solution, the ^{19}F NMR spectrum of [Fe(**1**)$(OTf)_2$] at RT exhibits a single, slightly broadened resonance around −20 ppm (see Table 4), which is consistent with the triflate anions existing as terminally coordinated ligands in a symmetrical cis-α geometry, as seen in the solid-state structure. The cyclohexyl derivative [Fe(**2**)$(OTf)_2$] shows a major, very broad signal at −5 ppm when measured at RT together with a minor (≈5%), sharp peak at −18 ppm (Figure 10). Upon cooling, the major peak splits into two signals, while the minor one remains unchanged. At 218 K, the two major peaks of equal intensity are observed at 39 and 12 ppm and the minor peak is observed at 1.6 ppm (the change in chemical shift is due to Curie-type behavior). The major species is assigned to a complex with cis-β geometry that results in two inequivalent triflate ligands, whereas the minor species is believed to have the cis-α geometry. This is supported by the ^1H NMR spectrum at this temperature, which shows ca. 20 major and ca. 10 minor peaks (Figure S13, Supporting Information). The ratio between the major and minor species does not appear to change with temperature, which suggests that the cis-α and cis-β geometries do not interconvert. At RT, the cis-β complex is labile and the triflate ligands are rapidly exchanging, whereas the minor cis-α complex is probably in a SC regime and much less labile, which results in a sharp ^{19}F NMR signal for these triflate ligands.

The ^{19}F NMR spectra in a CD_2Cl_2 solution of the complexes [Fe(**3**)$(OTf)_2$], [Fe(**4**)$(OTf)_2$], and [Fe(**5**)$(OTf)_2$] show very broad signals at RT, which upon cooling split into a multitude of peaks that could not be individually assigned (Figures S14, S15, and S16, Supporting Information).

In a CD_3CN solution, a single, prominent resonance is observed in the ^{19}F NMR spectra of complexes [Fe(**1**)$(OTf)_2$]−[Fe(**5**)$(OTf)_2$] at a chemical shift that is characteristic of free triflate anions (Table 4), which indicates that the species present in solution are in all cases a dicationic solvate complex $[Fe(L)(CD_3CN)_2]^{2+}$. For the fully HS complexes $[Fe(\mathbf{3})(CD_3CN)_2]^{2+}$, $[Fe(\mathbf{4})(CD_3CN)_2]^{2+}$, and $[Fe(\mathbf{5})(CD_3CN)_2]^{2+}$, this resonance is observed at ca. −69 ppm. This is downfield from the chemical shift values seen for truly free triflate anions (ca. −80 ppm), which indicates that there is a rapid equilibrium between the dication $[Fe(L)(CD_3CN)_2]^{2+}$ and triflate coordinated species, in which the former is predominant.

The ^{19}F NMR spectra in CD_3CN of the SC complexes [Fe(**1**)$(OTf)_2$] and [Fe(BPMEN)$(OTf)_2$] exhibit a prominent resonance at ca. −78 ppm. This seems to suggest that the only species present in solution is $[Fe(L)(CD_3CN)_2]^{2+}$ and that there is little or no fluxional exchange of the acetonitrile molecules and triflate anions. However, the corresponding ^1H NMR spectra show severe line-broadening that has been attributed to this exchange process (vide supra), which has been shown to be initiated by occupation of the HS manifold and to increase in speed as the SC region is traversed. Consequently, these SC complexes are expected to show very slow exchange with triflate anions, which is in contrast to the very rapid exchange exhibited by the fully HS complexes. This hypothesis was confirmed by the observation of a small, broad resonance at ca. −20 ppm in the ^{19}F NMR spectrum of complex [Fe(**1**)$(OTf)_2$] (Figure S18, Supporting Information). Upon re-examination of the ^{19}F NMR spectrum of the SC complex [Fe(BPMEN)$(OTf)_2$], a similar minor resonance was observed (Figure S17, Supporting Information). A chemical shift of this magnitude is characteristic of a terminally coordinated triflate anion and is most likely due to the monotriflate species $[Fe(L)(OTf)(CD_3CN)]^+$, which by integration of the corresponding ^{19}F resonances was found to constitute less than 5% of the total iron species present. The absence of a secondary resonance in the spectrum of [Fe(**2**)$(OTf)_2$] is most likely due to severe line-broadening resulting from the very rapid triflate−acetonitrile exchange process, which is caused by the complex [Fe(**2**)$(OTf)_2$] being at the upper boundary of the SC region at RT.

(41) Jones, V. A.; Sriprang, S.; Thornton-Pett, M.; Kee, T. P. *J. Organomet. Chem.* **1998**, *567*, 199−218.
(42) Burger, P.; Baumeister, J. M. *J. Organomet. Chem.* **1999**, *575*, 214−222.
(43) Mahon, M. F.; Whittlesey, M. K.; Wood, P. T. *Organometallics* **1999**, *18*, 4068−4074.
(44) Blakesley, D. W.; Payne, S. C.; Hagen, K. S. *Inorg. Chem.* **2000**, *39*, 1979−1989.
(45) Börzel, H.; Comba, P.; Hagen, K. S.; Lampeka, Y. D.; Lienke, A.; Linti, G.; Merz, M.; Pritzkow, H.; Tsymbal, L. V. *Inorg. Chim. Acta* **2002**, *337*, 407−419.

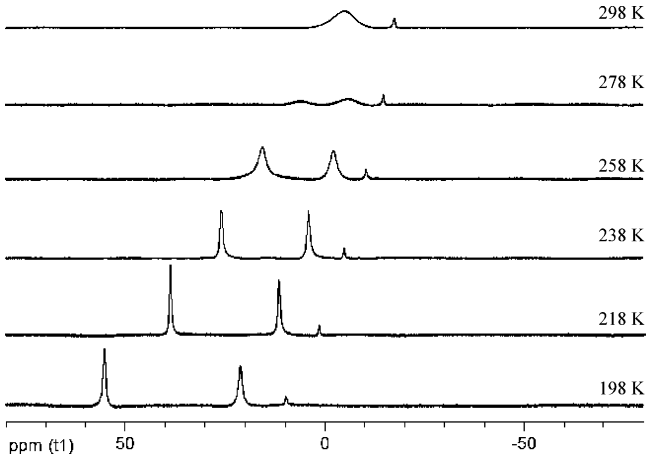

Figure 10. VT ^{19}F NMR spectra of complex [Fe(**2**)(OTf)$_2$] in CD_2Cl_2.

Geometrical Considerations. It is clear from the previous discussion of the geometries of the iron(II) complexes investigated here that the coordination geometries observed in the solid-state are not necessarily the same as those in a solution. In a solution, rapid equilibria can exist between different geometries, due to the labile nature of the metal complexes, in particular, with weakly coordinating triflate and acetonitrile ligands.

Bosnich and co-workers analyzed the relative stability of a series of Co(III) complexes containing the linear tetradentate tetraamine ligands 2,2,2-tet, 3,2,3-tet, and 2,3,2-tet, whereby the numbers denote the number of bridging atoms between the four amine donors.[46] The preference for any of the three possible topologies, cis-α, cis-β, or trans, depends on the cumulative bite-angle strain of the three chelate rings formed by the linear tetradentate ligand, which in turn is related to the absolute configuration of the chirality at the internal amine donors. Unlike the inert LS-d^6 Co(III) complexes, for which different conformational isomers can often be isolated, the labile HS-d^6 iron(II) complexes investigated here show rapid equilibria between different isomers, and the isomer that crystallizes preferentially may not be the dominant isomer in solution.

If we assume, once an iron(II) complex has been formed with a tetradentate bis(quinolyl) diamine ligand, that the absolute configuration of the internal amine donors is fixed, as being either *R* or *S*, and that only the outer quinolyl donors can dissociate and re-coordinate, then a series of equilibria can be proposed. In the case of an ethylene-bridged ligand, the absolute configuration at the amine N donor centers can be either the same (*R*,*R* or *S*,*S*) or different (*R*,*S* or *S*,*R*) and the central five-membered chelate can adopt either a "twist" or an "envelope" (sometimes called "half-chair") conformation (eqs 4 and 5).

In the case of complexes of **1** and BPMEN that feature three five-membered chelate rings, the cis-α (*R*,*R* or *S*,*S*) geometry with a twist conformation of the central chelate ring is the geometry seen in the solid-state (see Figure 3), and this conformation appears to be the most stable conformation in solution. In theory, a clockwise twist of 120° around one of the N−Fe bonds in the cis-α (*R*,*R*) isomer in eq 4, achieved by a dissociation and re-coordination of the co-ligands (triflate or acetonitrile), would result in the cis-β (*R*,*R*) topology together with an envelope conformation of the central five-membered chelate ring. Another twist around the other N−Fe bond would give the trans (*R*,*R*) topology. However, the latter two ligand rearrangements are highly unfavorable in the case of **1** and BPMEN due to the bite-angle strain; therefore, the only experimentally observed geometry is the cis-α (*R*,*R*) conformation.

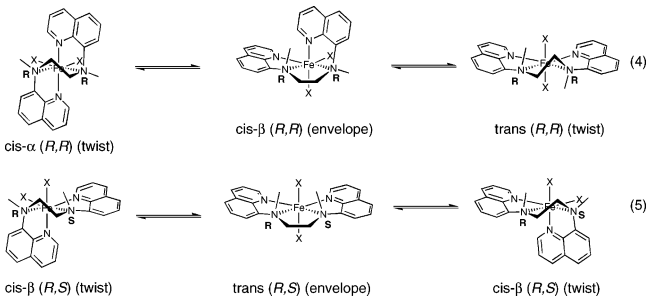

In the case of the cyclohexyl complex [Fe(BPMCN)(OTf)$_2$], both topological isomers, cis-α and cis-β, have been independently prepared.[24,47] The cis-α isomer has the same absolute configuration (*R*,*R* or *S*,*S*) at the amine donors, whereas different configurations (*R*,*S* or *S*,*R*) are seen in the cis-β isomer. In the complex [Fe(**2**)(OTf)$_2$], the predominant isomer (95% according to the VT ^{19}F NMR spectra, see Figure 10) adopts a cis-β conformation, whereas 5% has the cis-α geometry. On the basis of the close similarity of complex [Fe(**2**)(OTf)$_2$] with [Fe(BPMCN)(OTf)$_2$], this is likely to be a cis-β geometry with different configurations (*R*,*S* or *S*,*R*) at each amine donor. A cis-α (*R*,*S*) conformation is not possible, but a trans (*R*,S) conformation may be accessible, which would result in a dynamic interconversion between two cis-β geometries as shown in eq 5. This would explain the dynamic behavior seen for complex [Fe(**2**)(OTf)$_2$] in the VT ^{19}F NMR experiments. The small amount of an isomer with cis-α geometry (5%) observed for this complex likely has the same configuration (*R*,*R* or *S*,*S*) at each amine donor, again based on the similarity to the cis-α isomer of [Fe(BPMCN)(OTf)$_2$]. It is therefore also clear from these considerations that the two conformations cis-α (*R*,*R*) and cis-β (*R*,*S*) cannot interconvert, due to the different absolute configuration at the amine donors.

Ligand **5** in the complex [Fe(**5**)(OTf)$_2$] contains one central five-membered and two outer six-membered chelate rings. The increased flexibility of this ligand allows access to the cis-β (*R*,*R*) geometry (eq 4). In the X-ray analysis of a single crystal of complex [Fe(**5**)(OTf)$_2$], both the cis-β (*R*,*R*) and the cis-β (*R*,*S*) geometries are found in a 75/25 ratio, which crystallize together in this case (Figure 5 shows the cis-β (*S*,*S*) isomer and Figure S7 (Supporting Information) shows both isomers). The VT ^{19}F NMR spectrum in a CD_2Cl_2 solution shows a single broad peak at RT at −20 ppm. This peak splits into a multitude of signals at lower temperatures,

(46) Gavrilova, A. L.; Bosnich, B. *Chem. Rev.* **2004**, *104*, 349−383.

(47) Costas, M.; Tipton, A.; Chen, K.; Jo, D.-H.; Que, L., Jr. *J. Am. Chem. Soc.* **2001**, *123*, 6722−6723.

which indicates a fast equilibrium at RT, most likely between the two cis-β geometries and their corresponding trans geometries. Note that the trans (*R*,*R*) isomer is C_2 symmetric, giving rise to only one signal, whereas the trans (*R*,*S*) isomer is C_s symmetric (meso form) and features two inequivalent triflate anions. The order of relative stability for topological isomers of Co(III) complexes containing 3,2,3-tet ligands was determined by Bosnich to be as follows: trans (*R*,*R*) > cis-β (*R*,*R*) > cis-β (*R*,*S*) > trans (*R*,*S*) ≫ cis-α (*R*,*R*).[46]

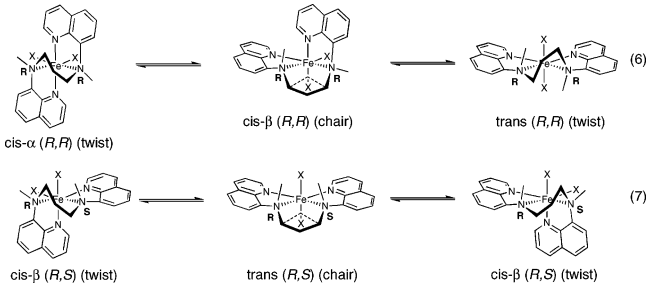

In the propyl-bridged complexes [Fe(**3**)(OTf)$_2$] and [Fe(**4**)(OTf)$_2$], the central chelate forms a six-membered ring, which can adopt either a twist or a chair conformation (or the less stable boat conformation, shown as a dashed line in eqs 6 and 7). The solid-state structure of complex [Fe(**4**)(OTf)$_2$] exhibits the cis-β (*R*,*R* or *S*,*S*) geometry, with a chair conformation of the central six-membered ring (Figure 4 shows the cis-β (*S*,*S*) isomer). The ^{19}F NMR spectra of [Fe(**3**)(OTf)$_2$] and [Fe(**4**)(OTf)$_2$] in a CD_2Cl_2 solution show broad resonances at RT, whereas at lower temperatures a multitude of peaks emerge, which indicates at least four different isomers in each case that could not be individually identified. The order of relative stability for topological isomers of Co(III) complexes containing 2,3,2-tet ligands is known to be as follows: trans (*R*,*S*) > trans (*R*,*R*) > cis-α (*R*,*R*) ≫ cis-β (*R*,*R*) and cis-β (*R*,*S*).[46] The solid-state structure of the iron(II) bis(triflate) complex of the propyl derivative of BPMEN, complex [Fe(BPMPN)(OTf)$_2$], was recently reported to have a trans (*R*,*S*) geometry, which is consistent with this order of stability.[40] The cis-α (*R*,*R*) geometry has been previously observed in the solid-state structure of the complex [Fe(BPMPN)Cl$_2$].[28] The observed cis-β (*R*,*R*) geometry for complex [Fe(**4**)(OTf)$_2$] is therefore somewhat surprising, but other factors may be responsible for the preferred crystallization of this particular isomer.

It is clear from this analysis that increasing the size of the chelate rings formed by linear tetradentate ligands increases the flexibility of these ligands and allows access to more than one geometry. Because of the labile nature of HS iron(II) complexes, several equilibria can exist between different topological isomers.

UV−vis Spectroscopy. The UV−vis spectra of ligands **1**−**5** are all characterized by high-intensity bands in the UV region (<300 nm) and a relatively intense band (ϵ_{max} = 8300−8600 M^{-1}·cm^{-1}) in the near visible region at λ_{max} = 350−380 nm (see Figure S19, Supporting Information), which is most likely due to $\pi-\pi^*$ transitions. This band is expected to shift to lower wavelength upon coordination to a metal center, as is seen in other 8-aminoquinoline complexes.[48] The UV−vis spectra of the iron(II) bis(triflate) complexes of the ligands **1**−**5** in acetonitrile are dominated by high-intensity bands in the UV region and broad transitions in the visible region (Figure 11 and Table 4). By analogy to spectra of similar iron(II) complexes of pyridinemethylamino ligands, these two sets of bands can be assigned to ligand-centered $\pi-\pi^*$ transitions (λ_{max} < 350 nm) and metal-to-ligand charge transfer (MLCT) bands between the iron(II) t_{2g} orbitals and the quinoline π^* orbitals, respectively.[49−52]

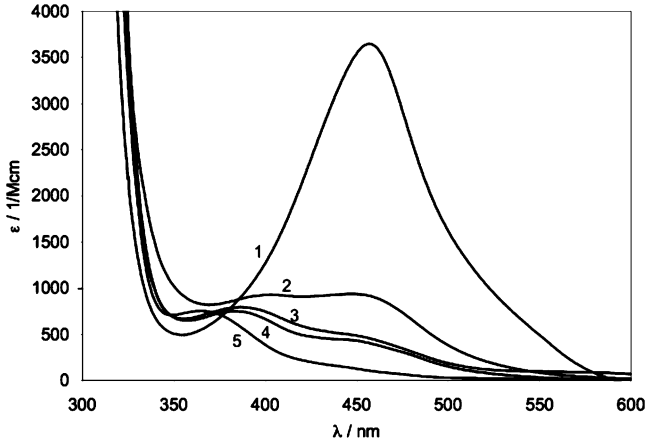

Figure 11. UV−vis spectra of iron bis(triflate) complexes in CH_3CN (*c* = 0.5 mM): (1) [Fe(**1**)(OTf)$_2$], (2) [Fe(**2**)(OTf)$_2$], (3) [Fe(**3**)(OTf)$_2$], (4) [Fe(**4**)(OTf)$_2$], and (5) [Fe(**5**)(OTf)$_2$].

One of the most noticeable facets of the UV−vis spectra in Figure 11 is that the extinction coefficient of the band centered at 456 nm (ϵ_{max} = 3600 M^{-1}·cm^{-1}) of complex [Fe(**1**)(OTf)$_2$] is significantly larger than those of the other complexes, for which ϵ_{max} varies between 440 and 940 M^{-1}·cm^{-1}. This, presumably, derives from the SC nature of this complex, which equates to an occupation of the LS configuration and, as in the case of complexes such as [Fe(BPMEN)(OTf)$_2$],[22] results in an enhancement of the MLCT band.[53] As might be expected, a minor enhancement is also observed for [Fe(**2**)(OTf)$_2$], which in acetonitrile and at RT shows residual occupation of the LS configuration (see Figure 6). The intensity of the MLCT band of the HS complexes [Fe(**3**)(OTf)$_2$], [Fe(**4**)(OTf)$_2$], and [Fe(**5**)(OTf)$_2$] is much weaker and the existence of multiple interconverting geometrical isomers in solution precludes further assignment.

Catalytic Oxidation of Cyclohexane. The catalytic properties of the iron(II) bis(triflate) complexes containing ligands **1**−**5** for the oxidation of cyclohexane with H_2O_2 have been evaluated (eq 8).

(48) Coakley, M. P. *Appl. Spectrosc.* **1964**, *18*, 149−152.
(49) Balland, V.; Banse, F.; Anxolabéhère-Mallart, E.; Nierlich, M.; Girerd, J.-J. *Eur. J. Inorg. Chem.* **2003**, 2529−2535.
(50) Borovik, A. S.; Papaefthymiou, V.; Taylor, L. F.; Anderson, O. P.; Que, L., Jr. *J. Am. Chem. Soc.* **1989**, *111*, 6183−6195.
(51) Toftlund, H. *Coord. Chem. Rev.* **1989**, *94*, 67−108.
(52) Mialane, P.; Nivorojkine, A.; Pratviel, G.; Azéma, L.; Slany, M.; Godde, F.; Simaan, A. J.; Banse, F.; Kargar-Grisel, T.; Bouchoux, G.; Sainton, J.; Horner, O.; Guilhem, J.; Tchertanova, L.; Meunier, B.; Girerd, J.-J. *Inorg. Chem.* **1999**, *38*, 1085−1092.
(53) Chang, H.-R.; McCusker, J. K.; Toftlund, H.; Wilson, S. R.; Trautwein, A.; Winkler, H.; Hendrickson, D. N. *J. Am. Chem. Soc.* **1990**, *112*, 6814−6827.

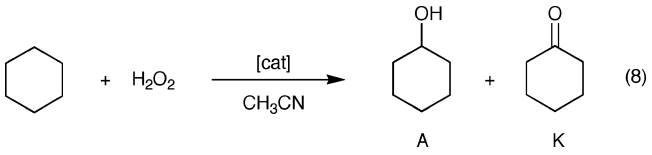

The oxidation reactions were carried out in acetonitrile as the solvent at RT under air. A hydrogen peroxide solution (70 mM, 10 equiv) was added to an acetonitrile solution containing the catalyst (2.1 μmol, 1 equiv) and cyclohexane (2.1 mmol, 1000 equiv). A large excess of substrate was used to minimize over-oxidation of cyclohexanol (A) to cyclohexanone (K). The addition of dilute H_2O_2 was carried out slowly using a syringe pump to minimize H_2O_2 decomposition. The yields are based on the amount of oxidant (H_2O_2) converted into oxygenated products. Two series of catalytic experiments were carried out initially, using 10 and 100 equiv of H_2O_2.

The iron bis(triflate) complex containing the ligand BPMEN was used as a benchmark against which the other catalysts were compared (see Table 6). The catalyst [Fe(BPMEN)$(OTf)_2$] converts 65% of the H_2O_2 added into oxygenated products with a large A/K ratio of 9.5. These results are consistent with those reported by Que and coworkers for the complex [Fe(BPMEN)$(CH_3CN)_2$]$(ClO_4)_2$.[13] The addition of more H_2O_2 (100 equiv) leads to a lower percentage conversion (48%) and a lower A/K ratio (2.5) due to over-oxidation of cyclohexanol to cyclohexanone. The series of bis(quinolyl) diamine complexes investigated here shows the following trends. Although not quite as effective as [Fe(BPMEN)$(OTf)_2$], the most active and selective catalyst is [Fe(**1**)$(OTf)_2$], with a conversion of 51% of H_2O_2 into product and an A/K ratio of 5.0 (30% and 2.3, respectively, at 100 equiv of H_2O_2). The propyl complexes [Fe(**3**)$(OTf)_2$] and [Fe(**4**)$(OTf)_2$] also show good activities and selectivities at 10 equiv, but their catalytic performance decreases significantly at 100 equiv of H_2O_2. Considering that these complexes are likely to exist as several interconverting geometrical isomers in solution, it is impossible to correlate these results in terms of structure−activity relationships. However, the initial high activity and subsequent drop in activity at higher H_2O_2 concentrations indicate that these catalysts are as active as [Fe(**1**)$(OTf)_2$], but they appear to decompose more readily. The activity measured with 10 equiv of H_2O_2 for complex [Fe(**2**)$(OTf)_2$], which exists mainly as the cis-β isomer, is significantly lower (16%) with an A/K ratio close to 1. Very low conversion (5%) with a low A/K ratio was also obtained in the case of [Fe(**5**)$(OTf)_2$]. The catalysts that give the highest conversions also appear to give the largest A/K ratios.

KIE values have been determined from competition experiments between C_6H_{12} and C_6D_{12} and were found to be between 2.5 and 4.5, which indicates that the reactions are mediated by a more selective metal-based oxidant than the unselective OH$^\bullet$ radical, for which a KIE of 1 is expected.[14] The 3°/2° C−H bond selectivities (normalized for the different numbers of secondary and tertiary C−H bonds, 12 and 4, respectively) from the oxidation of adamantane, using 70 mM (10 equiv) solutions of hydrogen peroxide in acetonitrile were also determined and values ranging from 10 to 16 were typically obtained. The unselective OH$^\bullet$ radicals typically afford values around 2, whereas more selective oxidants, as seen here, give substantially higher values.

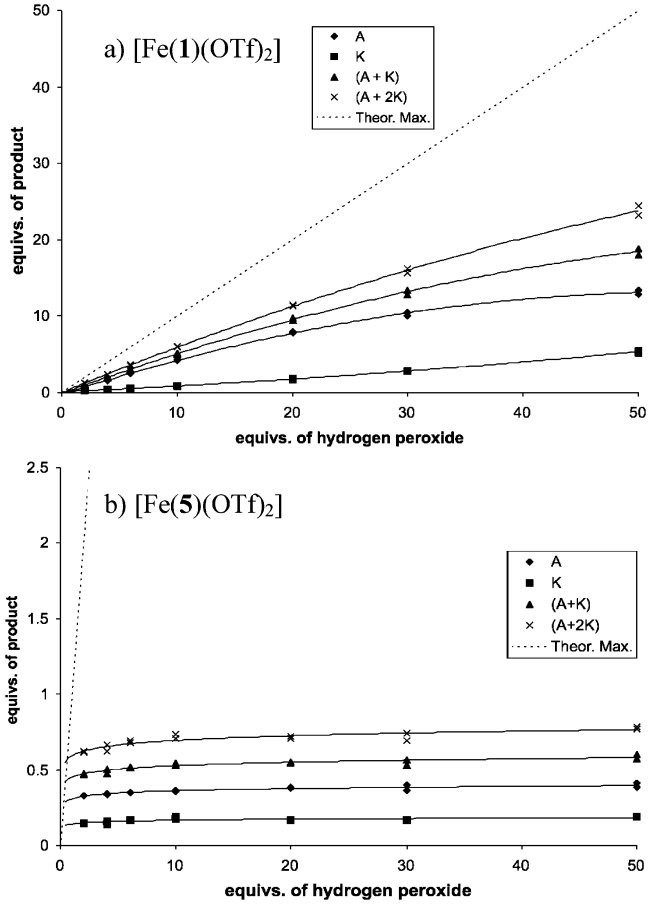

Figure 12. Product composition at various amounts of H_2O_2 in the oxidation of cyclohexane catalyzed by (a) [Fe(**1**)$(OTf)_2$] and (b) [Fe(**5**)$(OTf)_2$].

Table 6. Results for the Catalytic Oxidation of Cyclohexane[a]

run	complex	equiv H_2O_2	(A + K)[b] (%)	A/K[c]
1[d]	[Fe(BPMEN)$(OTf)_2$]	10	65	9.5
2[d]	[Fe(BPMEN)$(OTf)_2$]	100	48	2.5
3	[Fe(**1**)$(OTf)_2$]	10	51	5.0
4	[Fe(**1**)$(OTf)_2$]	100	30	2.3
5	[Fe(**2**)$(OTf)_2$]	10	16	1.1
6	[Fe(**2**)$(OTf)_2$]	100	9	1.5
7	[Fe(**3**)$(OTf)_2$]	10	49	4.4
8	[Fe(**3**)$(OTf)_2$]	100	15	2.9
9	[Fe(**4**)$(OTf)_2$]	10	34	2.1
10	[Fe(**4**)$(OTf)_2$]	100	9	1.8
11	[Fe(**5**)$(OTf)_2$]	10	5	1.7
12	[Fe(**5**)$(OTf)_2$]	100	1	1.5

[a] Catalytic conditions: see Experimental Procedures. [b] Total percentage yield of cyclohexanol (A) + cyclohexanone (K), expressed as moles of product per mole of H_2O_2. [c] Ratio of moles of cyclohexanol (A) to moles of cyclohexanone (K). [d] Previously determined, see reference 22.

The catalytic systems utilizing the complexes [Fe(**1**)$(OTf)_2$] and [Fe(**5**)$(OTf)_2$] were studied in more detail because they represent, respectively, the most and least active catalyst system studied here. The reaction profiles containing plots of the yields of A and K vs the equivalents of hydrogen

peroxide added, are given in Figure 12. All the individual catalytic runs were performed at least twice and a dashed diagonal line is included to represent the theoretical maximum yield (i.e., one mole of oxygenated product per mole of oxidant).

Upon examining the reaction profile for [Fe(**1**)$(OTf)_2$] (Figure 12a), it can be seen that the increase in the production of A observed upon the addition of increasing amounts of hydrogen peroxide deviates from linearity, whereas the production of K shows the opposite deviation (i.e., a decreasing A/K ratio). This is consistent with secondary oxidation of A to K, which increases in significance as the alcohol product builds up (cf. the 54% decrease in the A/K ratio observed upon moving from 70 to 700 mM hydrogen peroxide solutions in runs 3 and 4). With sufficient oxidant, cyclohexanone presumably would become the major product (A/K $<$ 1). This over-oxidation process can be viewed as nonproductive because it does not represent further conversion of cyclohexane to oxygenated product, which is reflected in the deviations of the molar (A+K) yield away from linearity in Figure 12a and in the 42% decrease in the percentage (A+K) yield observed upon moving from 70 to 700 mM solution (runs 3 and 4).

If we consider that a second equivalent of metal-based oxidant is required to oxidize the alcohol to ketone, then the number of equivalents of oxidant that has been used to generate the oxygenated products is given by the sum of the equivalents of alcoholic and twice the equivalents of ketonic products (A + 2K). Interestingly, the corresponding curve in Figure 12a shows a slight negative deviation from linearity, which seems to indicate that increasing the quantity of hydrogen peroxide added to the catalytic mixture causes a greater proportion of oxidant to be channelled into processes other than ketone and alcohol production. It was observed in the catalytic tests performed at higher hydrogen peroxide concentrations (700 mM) that the apparent drop in productivity seen with complex [Fe(**1**)$(OTf)_2$] is accompanied by the formation of small amounts of cyclohexyl hydroperoxide. This is consistent with an increased importance of autoxidation and is most likely a consequence of catalyst degradation, with the degradation product being responsible for the production of cyclohexyl hydroperoxide via Fenton-type chemistry.[3,10]

From the reaction profile of [Fe(**5**)$(OTf)_2$] (Figure 12b), it can be seen that this complex rapidly deactivates after the addition of the first few equivalents of hydrogen peroxide (i.e., one turnover at the metal center), which is probably due to a very fast degradation of the catalyst. Because the majority of the product was generated in the initial stages of the reaction, the high KIE and 3°/2° values (4.5 and 11 at 70 mM H_2O_2 concentration, respectively) represent the species present during this phase. This suggests that this complex is capable of forming metal-based oxidants during the first turnover, but the catalyst degradation products exhibit only residual autoxidative capacity. Consistent with this predicted trend, the KIE value measured for complex [Fe(**5**)$(OTf)_2$], under the standard catalyst testing conditions, upon increasing the hydrogen peroxide solution concentration from 70 to 700 mM decreased by only 22% from 4.5 to 3.5.

Conclusions

The solid-state and solution phase analysis of the series of bis(quinolyl)diamine iron(II) complexes investigated here has shown that, if the backbone of the tetradentate ligand is relatively small, for example, an ethylene bridge as in complex [Fe(**1**)$(OTf)_2$], the geometry in the solid-state and in solution is restricted to cis-α due to the formation of three five-membered chelate rings. This appears to give the strongest ligand field, such that the corresponding [Fe(**1**)-$(CH_3CN)_2]^{2+}$ complex is in a SC regime at RT. Changing the backbone to a cyclohexyl bridge such as ligand **2** restricts the NCCN dihedral angle of the backbone to 60°. This provides complex [Fe(**2**)$(OTf)_2$] with a cis-β coordination geometry, which is fluxional at RT in solution. The ligand field strength is reduced, as is indicated by the lower temperature for the onset of SC and the changes in the UV−vis spectrum. Increasing the size of the ligand backbone to propyl to give a six-membered central chelate ring, such as in complexes [Fe(**3**)$(OTf)_2$] and [Fe(**4**)$(OTf)_2$], results in an increased flexibility of the ligand. For complexes [Fe(**4**)-$(OTf)_2$] and [Fe(**5**)$(OTf)_2$], the solid-state geometry was found to be cis-β, but this does not represent the only geometry in solution. For these two complexes and also [Fe-(**3**)$(OTf)_2$], dynamic equilibria of complexes with different coordination geometries (cis-α, cis-β, and trans) are observed in solution by ^{19}F NMR spectroscopy. The magnetic moment measurements and the UV−vis spectra indicate that the ligand field strength in these three complexes is significantly reduced.

A high total percentage yield of alcohol and ketone (based upon moles of oxidant used) is generally accepted to be reflective of a catalyst's ability to facilitate hydrocarbon oxidation via non-autoxidative pathways. We have shown here, something we previously suspected,[22,25] that the stability, or the lack thereof, of the catalyst under reaction conditions is one of the primary factors limiting performance. Many of the complexes studied initially display reactivity that is characteristic of the formation of metal-based oxidants (i.e., high-valent iron oxo complexes), but they subsequently undergo degradation and then display only an ability to facilitate Fenton-type chemistry. The most stable, and by extension most successful, catalyst precursors that we have developed thus far have all shown a relatively strong ligand field and have exhibited at least partial occupation of the LS configuration. This maybe coincidental, but it seems more likely that the substitutional inertness of the LS manifold, which they are able to access, stabilizes the catalytic systems formed and thereby inhibits catalyst degradation.

Experimental Procedures

General. All moisture- and oxygen-sensitive compounds were prepared using a standard high vacuum line, Schlenk, or cannula techniques. A standard nitrogen-filled glove box was used for any subsequent manipulation and storage of these compounds. Standard ^1H, ^{19}F, and ^{13}C NMR spectra were recorded at 298 K using a

Bruker AC-250 MHz spectrometer. VT−NMR and COSY spectra were recorded using a Bruker AM-500 MHz or a DRX-400 MHz spectrometer. The ^{1}H and ^{13}C NMR chemical shifts were referenced to the residual protio impurity and ^{13}C NMR signal of the deuterated solvent, respectively. The ^{19}F NMR chemical shifts were referenced to $CFCl_3$. Mass spectra were recorded using either a VG Autospec or a VG Platform II spectrometer. Elemental analyses were performed by the Science Technical Support Unit at The London Metropolitan University. Gas chromatography (GC) analysis was performed using an Agilent 6890A gas chromatograph on either a HP-5 (30 m × 0.32 mm, film thickness 0.25 μm) or an Innowax (30 m × 0.25 mm, film thickness 0.25 μm) column. Toluene was used as the standard for quantitative analysis, and product identities were confirmed using GC-mass spectroscopy (GC-MS). UV−vis spectra were recorded at 298 K in an acetonitrile solution using a Perkin-Elmer Lambda 20 spectrometer.

Solvents and Reagents. Diethyl ether and tetrahydrofuran were dried by prolonged reflux under a nitrogen atmosphere and over sodium metal with a benzephenone ketyl indicator. They also were freshly distilled prior to use. Dichloromethane (DCM) and acetonitrile were treated in a similar manner, but calcium hydride was used as the drying agent. Toluene and pentane were dried by passing each through a column that was packed with commercially available Q-5 reagent (13% CuO on alumina) and activated alumina (pellets, 3 mm) in a stream of nitrogen. $Fe(OTf)_2(CH_3CN)_2$,[54] [Fe(BPMEN)-$(OTf)_2$],[22] [Fe(BPMEN)$(CH_3CN)_2$]$(ClO_4)_2$,[23] 8-formylquinoline,[55] and *N*-methyl-8-aminoquinoline[56] were all prepared according to published procedures.

***N,N′*-Bis(8-quinolyl)ethane-1,2-diamine:** A mixture of 8-hydroxyquinoline (50.0 g, 344 mmol), ethylene-1,2-diamine (11.5 mL, 172 mmol), sodium metabisulfite (65.6 g, 344 mmol), and water (350 mL) was stirred at reflux for 8 days. Upon cooling, the solution was made strongly alkaline (pH ≥ 12) by the addition of sodium hydroxide. The resulting mixture was cooled to RT and then filtered. The solid was extracted twice with DCM (400 mL), and the DCM extracts were combined, dried ($MgSO_4$), and the solvent was removed using the rotary evaporator. The solid obtained was triturated with hot ethanol (100 mL), filtered, and air-dried to give a yellow solid (24.2 g, 45%). ^{1}H NMR ($CDCl_3$): δ 8.70 (d, 2H, J = 4 Hz, 2-Qn*H*), 8.06 (d, 2H, J = 8 Hz, 4-Qn*H*), 7.39 (m, 4H, 3-Qn*H* and 6-Qn*H*), 7.08 (d, 2H, J = 8 Hz, 5-Qn*H*), 6.78 (d, 2H, J = 8 Hz, 7-Qn*H*), 6.44 (s, 2H, N*H*), 3.76 (s, 4H, NCH_2). ^{13}C NMR ($CDCl_3$): δ 146.9, 144.7 (*ipso*), 138.3 (*ipso*), 136.0, 128.7 (*ipso*), 127.7, 121.4, 114.2, 104.7, 42.8 (NCH_2). MS (+EI): *m*/*z* (%) 314 (7) [M$^+$], 170 (48) [(M − QnNH$_2$)$^+$], 157 (100) [(QnNHCH$_2$)$^+$], 144 (15) [(QnNH$_2$)$^+$], 129 (26) [(QnH)$^+$]. Anal. Calcd. (found) for $C_{24}H_{26}N_4$: C, 76.41 (76.30); H, 5.77 (5.62); N, 17.82 (17.73).

***N,N′*-Dimethyl-*N,N′*-bis(8-quinolyl)ethane-1,2-diamine (1):** Eight milliliters (12.7 mmol) of 1.6 M *n*-butyl lithium in hexanes was added dropwise to a solution of 2.0 g (6.36 mmol) of *N*,*N*′-bis(8-quinolyl)ethane-1,2-diamine in THF (75 mL). The mixture was cooled to −78 °C and stirred at −78 °C for 1 h, followed by an additional hour of mixing at RT to give a dark, red-brown solution. This resulting solution was then cooled to −78 °C and 4.0 mL (63.6 mmol) of methyl iodide was added, after which the cooling bath was removed and the reaction mixture was stirred for an additional 12 h. Subsequent to this mixing period, a saturated aqueous sodium hydrogen carbonate solution and diethyl ether were added to the mixture. Separation of the organic layer was followed by extraction of the aqueous layer with DCM (2 × 100 mL). The organic fractions were combined, dried ($MgSO_4$), and the solvent was removed using the rotary evaporator. Purification of the solid obtained by recrystallization from ethanol gave (**1**) as a crystalline, pale yellow-brown solid (1.59 g, 73%). ^{1}H NMR ($CDCl_3$): δ 8.75 (d, 2H, J = 4 Hz, 2-Qn*H*), 8.05 (d, 2H, J = 8 Hz, 4-Qn*H*), 7.31 (m, 6H, 3-, 5-, and 6-Qn*H*), 7.04 (d, 2H, J = 8 Hz, 7-Qn*H*), 3.95 (s, 4H, NCH_2), 3.06 (s, 6H, N*Me*). ^{13}C NMR ($CDCl_3$): δ 149.2 (*ipso*), 147.2, 142.5(*ipso*), 136.2, 129.6, 126.5, 120.7, 119.8, 115.5, 54.0 (NCH_2), 41.2 (N*Me*). MS (+EI): *m*/*z* (%) 342 (0.4) [M$^+$], 298 (0.8) [(M − (Me)(Et))$^+$], 184 (66) [(M − (Qn)$(CH_3)_2$)$^+$], 171 (100) [(QnNMeCH$_2$)$^+$], 158 (49) [(QnNHMe)$^+$], 129 (45) [(QnH)$^+$]. Anal. Calcd. (found) for $C_{22}H_{22}N_4$: C, 77.16 (76.91); H, 6.48 (6.63); N, 16.36 (16.23).

***N,N′*-Bis(8-quinolyl)cyclohexane-diamine:** A mixture of 14.5 g (100 mmol) of 8-hydroxyquinoline, 6.0 mL (50 mmol) of *trans*-diaminocyclohexane, 19.0 g (100 mmol) of sodium metabisulfite, and 500 mL of water was heated at reflux for 7 days. Subsequent to cooling, the solution was made strongly alkaline (pH ≥ 12) by the addition of sodium hydroxide. The resultant mixture was extracted twice with DCM (50 mL), dried ($MgSO_4$), and reduced to dryness using a rotary evaporator. The solid obtained was recrystallized from ethanol to give a pale yellow crystalline solid (5.1 g, 28%). ^{1}H NMR ($CDCl_3$): δ 8.57 (d, 2H, J = 4 Hz, 2-Qn*H*), 7.98 (d, 2H, J = 8 Hz, 4-Qn*H*), 7.32 (m, 4H, 3-Qn*H* and 6-Qn*H*), 6.98 (d, 2H, J = 8 Hz, 5-Qn*H*), 6.82 (d, 2H, J = 8 Hz, 7-Qn*H*), 6.41 (d, 2H, J = 7 Hz, N*H*), 3.77 (m, 2H, NC*H*), 2.41 (m, 2H, C*H*), 1.86 (m, 2H, C*H*), 1.56 (m, 4H, CH_2). All other analytical data have been previously reported.[57]

***N,N′*-Dimethyl-*N,N′*-bis(8-quinolyl)cyclohexane-diamine (2):** Synthesis was carried out from 5.1 mL (8.16 mmol) of 1.6 M *n*-butyl lithium in hexanes, 1.5 g (4.08 mmol) of *N*,*N*′-bis(8-quinolyl)cyclohexane-diamine and 2.5 mL (40.8 mmol) of methyl iodide via a procedure analogous to that used in the preparation of **1** to give **2** as an orange microcrystalline solid (1.00 g, 64%). ^{1}H NMR ($CDCl_3$): δ 8.81 (d, 2H, J = 4 Hz, 2-Qn*H*), 8.08 (d, 2H, J = 8 Hz, 4-Qn*H*), 7.35 (m, 4H, 3-Qn*H* and 6-Qn*H*), 7.22 (m, 2H, J = 8 Hz, 5-Qn*H*), 6.69 (d, 2H, J = 8 Hz, 7-Qn*H*), 4.79 (m, 2H, NC*H*), 2.52 (s, 6H, N*Me*), 2.39 (m, 2H, C*H*), 1.84 (m, 2H, C*H*), 1.71 (m, 2H, C*H*), 1.40 (m, 2H, C*H*). ^{13}C NMR ($CDCl_3$): δ 149.4 (*ipso*), 146.3, 142.3 (*ipso*), 136.2, 129.7 (*ipso*), 126.7, 120.4, 117.7, 115.4, 63.2 (NCH), 33.6 (N*Me*), 30.3 (NCH*C*H$_2$), 26.0 (NCHCH$_2$*C*H$_2$). MS (+EI): *m*/*z* (%) 396 (22) [M$^+$], 238 (100) [(M − (QnNHMe))$^+$], 223 (22) [(M − (QnNHMe$_2$))$^+$], 209 (24) [(M − (QnNHMeEt))$^+$], 197 (20) [(QnN$(CH_3)(C_3H_4)$)$^+$], 183 (27) [(QnN$(CH_2)(C_2H_3)$)$^+$], 171 (34) [(QnNMeCH$_2$)$^+$], 157 (28) [(QnNHMe)$^+$], 129 (33) [(QnH)$^+$]. Anal. Calcd. (found) for $C_{26}H_{28}N_4$: C, 78.75 (78.42); H, 7.12 (7.13); N, 14.13 (14.07).

***N,N′*-Bis(8-quinolyl)-2,2-dimethylpropane-1,3-diamine:** This compound was prepared in a fashion analogous to the cyclohexyl derivative using 7.26 g (50 mmol) of 8-hydroxyquinoline, 3.0 mL (25 mmol) of 2,2-dimethyl-1,3-diaminopropane, 9.5 g (50 mmol) of sodium metabisulfite, and 300 mL of water. The resulting residue was triturated with cold ethanol and was dried under vacuum to give a yellow oil (3.1 g, 35%). ^{1}H NMR ($CDCl_3$): δ 8.69 (d, 2H, J = 4 Hz, 2-Qn*H*), 8.04 (d, 2H, J = 8 Hz, 4-Qn*H*), 7.34 (m, 4H, 3-Qn*H* and 6-Qn*H*), 7.01 (d, 2H, J = 8 Hz, 5-Qn*H*), 6.73 (d, 2H, J = 7 Hz, 7-Qn*H*), 6.47 (t, 2H, J = 6 Hz, N*H*), 3.37 (d, 4H, J = 6 Hz, NCH_2), 1.28 (s, 6H, C*Me*). ^{13}C NMR ($CDCl_3$): δ 146.7,

(54) Hagen, K. S. *Inorg. Chem.* **2000**, *39*, 5867−5869.
(55) Seyhan, M.; Fernelius, W. C. *J. Org. Chem.* **1957**, *22*, 217.
(56) Deady, L. W.; Yusoff, N. L. *J. Heterocycl. Chem.* **1976**, *13*, 125−126.
(57) Suzuki, T. M.; Kamiyama, S.; Kimura, T. *Bull. Chem. Soc. Jpn.* **1978**, *51*, 1094−1097.

145.5 (*ipso*), 138.3 (*ipso*), 135.9, 128.7 (*ipso*), 127.8, 121.3, 113.4, 104.6, 52.0 (NCH_2), 37.0 (*C*Me), 24.3 (C*Me*).

***N,N′*-Dimethyl-*N,N′*-bis(8-quinolyl)-2,2-dimethylpropane-1,3-diamine (3):** This compound was prepared from 1.8 mL (2.92 mmol) of 1.6 M *n*-butyl lithium in hexanes, 0.52 g (1.46 mmol) of *N,N′*-bis(8-quinolyl)-2,2-dimethylpropane-1,3-diamine, and 0.9 mL (14.6 mmol) of methyl iodide via a procedure analogous to that used in the synthesis of **1**. Purification performed by flash column chromatography using a 50:50 ethyl acetate/petroleum ether (40−60 °C) solvent mixture gave **3** as a yellow oil (0.30 g, 53%). ^{1}H NMR ($CDCl_3$): δ 8.78 (d, 2H, J = 4 Hz, 2-Qn*H*), 8.06 (d, 2H, J = 8 Hz, 4-Qn*H*), 7.28 (m, 6H, 3-Qn*H*, 6-Qn*H* and 5-Qn*H*), 7.10 (d, 2H, J = 8 Hz, 7-Qn*H*), 3.81 (s, 4H, NCH_2), 3.19 (s, 6H, N*Me*), 0.73 (s, 6H, C*Me*). ^{13}C NMR ($CDCl_3$): δ 150.2 (*ipso*), 146.7, 142.8 (*ipso*), 136.3, 129.8 (*ipso*), 126.6, 120.5, 119.5, 117.6, 64.4 (N*C*H_2), 45.9 (N*Me*), 43.8 (NCH$_2$*C*Me), 25.7 (NCH$_2$C*Me*).

***N,N′*-Dimethyl-*N,N′*-bis(8-quinolyl)propane-1,3-diamine 4:** The 3.95 mL (6.32 mmol) portion of 1.6 M *n*-butyl lithium in hexanes was added dropwise to a solution of N-methyl-8-aminoquinoline (1.00 g, 6.32 mmol) in THF (75 mL), and the mixture was cooled to −78 °C. The dark red solution that was obtained was stirred for 1 h at −78 °C and subsequently at RT for an additional hour. The mixture was re-cooled to −78 °C and 0.37 mL (3.66 mmol) of 1,3-dibromopropane was added. The cooling bath was then removed, and the mixture was allowed to stir for an additional 12 h. The reaction was quenched by the addition of 30 mL of aqueous hydrogen carbonate solution. An extraction was performed using DCM (3 × 30 mL). The organic layers were combined, dried ($MgSO_4$), and the solvent was removed using a rotary evaporator to yield a brown oil. Purification by flash column chromatography was performed using a 50:50 ethyl acetate/petroleum ether (40−60 °C) solvent mixture to give **4** as a yellow oil (0.56 g, 43%). ^{1}H NMR ($CDCl_3$): δ 8.78 (d, 2H, J = 4 Hz, 2-Qn*H*), 8.05 (d, 2H, J = 8 Hz, 4-Qn*H*), 7.31 (m, 6H, 3-Qn*H*, 6-Qn*H* and 5-Qn*H*), 7.04 (m, 2H, 7-Qn*H*), 3.55 (t, 4H, J = 8 Hz, NCH_2), 3.00 (s, 6H, N*Me*), 2.02 (q, 2H, J = 8 Hz, NCH$_2$CH_2). ^{13}C NMR ($CDCl_3$): δ 149.4 (*ipso*), 147.6, 142.9 (*ipso*), 136.2, 129.6 (*ipso*), 126.5, 120.7, 120.4, 116.5, 54.3 (N*C*H_2), 41.3 (N*Me*), 24.4 (NCH$_2$*C*H$_2$).

***N,N′*-Dimethyl-*N,N′*-bis(8-quinolylmethyl)ethane-1,2-diamine (5):** A solution of 8-formylquinoline (1.20 g, 7.64 mmol) in DCM (25 mL) was added to a vigorously stirring mixture of *N,N′*-dimethylethylene-1,2-diamine (0.40 mL, 3.78 mmol) and sodium triacetoxyborohydride (3.40 g, 16.0 mmol) in DCM (100 mL). The combined mixture was allowed to stir for 12 h. The reaction mixture was quenched by the addition of a saturated sodium hydrogen carbonate solution and the product was extracted with ethyl acetate (3 × 100 mL). The organic fractions were combined, dried ($MgSO_4$), and the solvent was removed using the rotary evaporator. The yellow oil that was obtained was reacted with 1 equiv (0.34 g, 3.78 mmol) of oxalic acid in methanol (25 mL) to give a white precipitate. This oxalate salt was isolated by filtration, washed with small quantities of cold methanol (2 × 5 mL), and allowed to air-dry. It was then treated with an aqueous 3 M NaOH solution, and the resultant mixture was extracted with DCM (3 × 100 mL). The organic layers were combined, dried ($MgSO_4$), and the solvent was removed using the rotary evaporator to give **5** as a viscous yellow oil (1.11 g, 79%). ^{1}H NMR ($CDCl_3$): δ 8.90 (d, 2H, J = 3 Hz, 2-Qn*H*), 8.12 (d, 2H, J = 8 Hz, 4-Qn*H*), 7.89 (d, 2H, J = 7 Hz, 5-Qn*H*), 7.69 (d, 2H, J = 8 Hz, 7-Qn*H*), 7.46 (t, 2H, J = 8 Hz, 6-Qn*H*), 7.37 (dd, 2H, J = 4 Hz and J = 8 Hz, 3-Qn*H*), 4.28 (s, 4H, QnCH_2), 2.83 (s, 4H, NCH_2CH_2N), 2.37 (s, 6H, N*Me*). ^{13}C NMR ($CDCl_3$): δ 162.6, 161.7 (*ipso*), 137.4 (*ipso*), 136.3, 129.2, 128.2 (*ipso*), 126.5, 126.3, 120.7, 57.1 (Qn*C*H_2), 56.2 (N*C*H_2*C*H_2N), 43.4 (N*Me*). MS (+EI): *m*/*z* (%) 198 (8) [(M-QnCH$_2$NHCH$_3$)$^+$], 185 (80) [(QnCH$_2$NmeCH$_2$)$^+$], 157 (7) [(QnCH$_2$NH)$^+$], 142 (100) [(QnMe)$^+$], 129 (9) [(QnH)$^+$], 115 (8) [(Me$_2$NCH$_2$CH$_2$NMeCH$_2$)$^+$].

***N,N′*-Dimethyl-*N,N′*-bis(8-quinolyl)ethane-1,2-diamine Iron-(II) bis(triflate) [Fe(1)(OTf)$_2$]:** Sixty milliliters of THF was added to a Schlenk flask containing 0.80 g (2.34 mmol) of **1** and 1.02 g (2.34 mmol) of Fe(OTf)$_2$(CH$_3$CN)$_2$, and the resulting mixture was stirred overnight. The precipitate that formed during this time was isolated by reduction of the volume of THF to approximately 10 mL, followed by filtration. Subsequently, this solid was washed twice with small volumes of THF, once with diethyl ether, and then dried under a vacuum to give a voluminous orange powder (1.33 g, 82%). Crystals suitable for X-ray analysis were grown by slow diffusion from a concentrated DCM solution layered with pentane. ^{1}H NMR (CD_2Cl_2, all peaks appear as broad singlets): δ 72.2 (6H, N*Me*), 51.3 (2H, 2-Qn*H*), 29.0 (2H, 3-Qn*H*), 18.0 (2H, 5-Qn*H*), 17.5 (2H, 7-Qn*H*), 11.8 (2H, 6-Qn*H*), 2.0 (2H, 4-Qn*H*). ^{1}H NMR (CD_3CN, all peaks appear as broad singlets): δ 48.7 (2H, H_A), 31.2 (2H, 2-Qn*H*), 25.2 (6H, N*Me*), 19.6 (2H, 3-Qn*H*), 17.0 (2H, H_B), 12.8 (6H, 5-Qn*H*, 6-Qn*H* and 7-Qn*H*), 2.3 (2H, 4-Qn*H*). ^{19}F−NMR (CD_2Cl_2): δ −25.1 ($\nu_{1/2}$ = 820 Hz). ^{19}F−NMR (CD_3CN): δ −78.1 ($\nu_{1/2}$ = 720 Hz). MS (+FAB): *m*/*z* 696 [M$^+$], 547 [(M − OTf)$^+$]. Anal. Calcd. (found) for $C_{24}H_{22}F_6FeN_4O_6S_2$: C, 41.39 (41.31); H, 3.18 (3.03); N, 8.05 (7.90). μ_{eff} (CD_2Cl_2) = 5.39 μ_B. μ_{eff} (CD_3CN) = 3.72 μ_B.

***N,N′*-Dimethyl-*N,N′*-bis(8-quinolyl)cyclohexane-diamine Iron-(II) Bis(triflate) [Fe(2)(OTf)$_2$]:** Preparation from 0.39 g (0.99 mmol) of **2** and 0.43 g (0.99 mmol) of Fe(OTf)$_2$(CH$_3$CN)$_2$ was performed via a synthetic procedure analogous to that used in the production of [Fe(**1**)(OTf)$_2$] to give a yellow powder (0.44 g, 58%). ^{1}H NMR (CD_3CN, all peaks appear as broad singlets): δ 92.1 (3H, N*Me*), 72.0 (3H, N*Me*), 57.2 (1H), 46.5 (1H), 39.0 (1H), 31.7 (1H), 21.5 (1H), 20.6 (1H), 19.5 (1H), 16.3 (1H), 13.8 (1H), 12.9 (2H), 7.9 (1H), 4.7, 3.7, −0.8, −10.2 (1H), −20.9 (1H). ^{19}F−NMR (CD_2Cl_2): δ −5.4 (95%, $\nu_{1/2}$ = 2300 Hz) −17.6 (5%, $\nu_{1/2}$ = 200 Hz). ^{19}F−NMR (CD_3CN): δ −76.6 ($\nu_{1/2}$ = 2970 Hz). MS (+FAB): *m*/*z* 750 [M$^+$], 601 [(M − OTf)$^+$]. Anal. Calcd. (found) for $C_{26}H_{28}F_6FeN_4O_6S_2$: C, 44.81 (44.75); H, 3.76 (3.85); N, 7.47 (7.34). μ_{eff} (CD_2Cl_2) = 4.9 μ_B. μ_{eff} (CD_3CN) = 5.4 μ_B.

***N,N′*-Dimethyl-*N,N′*-bis(8-quinolyl)-2,2-dimethylpropane-1,3-diamine Iron(II) Bis(triflate) [Fe(3)(OTf)$_2$]:** A solution of **3** (0.25 g, 0.65 mmol) in THF (20 mL) was added to a stirring solution of Fe(OTf)$_2$(CH$_3$CN)$_2$ (0.28 g, 0.65 mmol) in THF (10 mL). A precipitate began to form within minutes. The mixture was stirred overnight, after which the volume of THF was reduced to approximately 10 mL, and then the mixture was filtered. The solid obtained was washed twice with small volumes of THF, once with diethyl ether, and then dried under a vacuum to give a yellow powder (0.25 g, 52%). ^{1}H NMR (CD_3CN, all peaks appear as broad singlets): δ 42.9 (2H, NCH_2), 40.3 (br, 6H, NMe), 28.5 (2H, 2-Qn*H*), 25.9 (2H, 3-Qn*H*), 21.6 (2H, NCH_2), 8.3 (6H, 5,6,7-Qn*H*), −2.1 (2H, 4-Qn*H*). ^{19}F−NMR (CD_2Cl_2): δ −17 ($\nu_{1/2}$ = 1500 Hz). ^{19}F−NMR (CD_3CN): δ −68.1 ($\nu_{1/2}$ = 2640 Hz). MS (+FAB): *m*/*z* 738 [M$^+$], 589 [(M − OTf)$^+$]. Anal. Calcd. (found) for $C_{27}H_{28}F_6FeN_4O_6S_2$: C, 43.91 (43.92); H, 3.82 (3.78); N, 7.59 (7.52). μ_{eff} (CD_2Cl_2) = 5.2 μ_B. μ_{eff} (CD_3CN) = 5.5 μ_B.

***N,N′*-Dimethyl-*N,N′*-bis(8-quinolyl)propane-1,3-diamine Iron-(II) Bis(triflate) [Fe(4)(OTf)$_2$]:** Preparation from 0.23 g (0.63 mmol) of **4** and 0.27 g (0.63 mmol)of Fe(OTf)$_2$(CH$_3$CN)$_2$ was performed via a synthetic procedure analogous to that used in the production of [Fe(**3**)(OTf)$_2$] to give a pale yellow powder (0.28 g, 62%). Crystals suitable for X-ray diffraction were grown by slow

Table 7. Crystallographic Data for Complexes [Fe(**1**)(OTf)$_2$], [Fe(**4**)(OTf)$_2$], and [Fe(**5**)(OTf)$_2$][a]

data	[Fe(**1**)(OTf)$_2$]	[Fe(**4**)(OTf)$_2$]	[Fe(**5**)(OTf)$_2$]
chemical formula	$C_{24}H_{22}F_6FeN_4O_6S_2$	$C_{25}H_{24}F_6FeN_4O_6S_2$	$C_{26}H_{26}F_6FeN_4O_6S_2$
solvent			CH_2Cl_2
fw	696.43	710.45	809.40
T (°C)	−100	−70	−100
space group	$P2_12_12_1$ (No. 19)	$P\bar{1}$ (No. 2)	$P2_1/c$ (No. 14)
a (Å)	9.5484(3)	9.6140(4)	10.8900(5)
b (Å)	13.5201(4)	16.8170(7)	15.6607(6)
c (Å)	21.4401(7)	19.3532(7)	19.3970(10)
α (deg)		73.806(3)	
β (deg)		78.501(3)	98.309(4)
γ (deg)		80.900(3)	
V (Å^3)	2767.82(15)	2927.0(2)	3273.3(3)
Z	4	4[b]	4
ρ_{calcd} (g·cm^{-3})	1.671	1.612	1.642
λ (Å)	0.71073	0.71073	0.71073
μ (mm^{-1})	0.784	0.743	0.833
R_1[c]	0.039	0.046	0.085
wR_2[d]	0.084	0.115	0.218

[a] Oxford Diffraction Xcalibur 3 diffractometer, graphite monochromated Mo−Kα radiation, refinement based on F^2. [b] There are two crystallographically independent molecules in the asymmetric unit. [c] $R_1 = \sum||F_o| - |F_c||/\sum|F_o|$. [d] $wR_2 = \{\sum[w(F_o^2 - F_c^2)^2]/\sum[w(F_o^2)^2]\}^{1/2}$; $w^{-1} = \sigma^2(F_o^2) + (aP)^2 + bP$.

diffusion from a DCM solution layered with pentane. ^{1}H NMR (CD_3CN, all peaks appear as broad singlets): δ 84.0 (6H, N*Me*), 46.3 (2H, NCH_2CH$_2$), 29.4 (2H, 2-Qn*H*), 24.4 (2H, 3-Qn*H*), 17.3 (2H, NCH_2CH$_2$), 0.8 (2H, 4-Qn*H*), −28.5 (2H, NCH$_2$CH_2). ^{19}F−NMR (CD_2Cl_2): δ −5.4 (40%, $\nu_{1/2}$ = 1500 Hz) −17.1 (60%, $\nu_{1/2}$ = 3000 Hz). ^{19}F−NMR (CD_3CN): δ −69.7 ($\nu_{1/2}$ = 1570 Hz). MS (+FAB): *m*/*z* 710 [M$^+$], 561 [(M − OTf)$^+$]. Anal. Calcd. (found) for $C_{25}H_{24}F_6FeN_4O_6S_2$: C, 42.27 (42.18); H, 3.41 (3.31); N, 7.89 (7.86). μ_{eff} (CD_2Cl_2) = 4.9 μ_B. μ_{eff} (CD_3CN) = 5.0 μ_B.

***N,N′*-Dimethyl-*N,N′*-bis(8-quinolylmethyl)ethane-1,2-diamine Iron(II) Bis(triflate) [Fe(5)(OTf)$_2$]:** Preparation from 1.04 g (2.81 mmol) of **5** and 1.10 g (2.53 mmol) of Fe(OTf)$_2$(CH$_3$CN)$_2$ was performed via a synthetic procedure analogous to that used in the production of [Fe(**3**)(OTf)$_2$] to give a yellow powder (1.52 g, 83%). Crystals suitable for X-ray diffraction were grown by slow diffusion from a DCM solution layered with pentane. ^{1}H NMR (CD_3CN, all peaks appear as broad singlets): δ 79.6 (2H, 2-Qn*H*), 37.1 (2H, *H*$_C$), 32.1 (2H, *H*$_D$), 26.7 (2H, 3-Qn*H*), 24.7 (2H, 6-Qn*H*), 22.9 (2H, *H*$_A$), 18.1 (2H, *H*$_B$), 14.1 (2H, 4-Qn*H*), 11.2 (2H, 5-Qn*H*), 8.8 (2H, 7-Qn*H*), 4.3, 3.9. ^{19}F−NMR (CD_2Cl_2): δ −19.9 ($\nu_{1/2}$ = 1500 Hz). ^{19}F−NMR (CD_3CN): δ −69.8 ($\nu_{1/2}$ = 210 Hz). MS (+FAB): *m*/*z* 724 [M$^+$], 575 [(M − OTf)$^+$]. Anal. Calcd. (found) for $C_{26}H_{26}F_6FeN_4O_6S_2$: C, 43.11 (43.20); H, 3.62 (3.47); N, 7.73 (7.63). μ_{eff} (CD_2Cl_2) = 4.86 μ_B. μ_{eff} (CD_3CN) = 5.06 μ_B.

***N,N′*-Dimethyl-*N,N′*-bis(8-quinolyl)ethylene-1,2-diamine Iron(II) Bis(acetonitrile) Perchlorate [Fe(1)(CH$_3$CN)$_2$](ClO$_4$)$_2$:** Twenty-five milliliters of acetonitrile were added to a Schlenk flask containing 1 equiv each of **1** (0.20 g, 0.58 mmol) and Fe(ClO$_4$)$_2$·*n*H$_2$O (0.15 g, 0.58 mmol), and the resulting mixture was stirred overnight. Subsequently, the volume of the solvent was reduced under a vacuum and diethyl ether was added to precipitate a solid. This solid was washed with diethyl ether, briefly dried under vacuum, and purified by slow diffusion recrystallization from a concentrated acetonitrile solution layered with pentane to give an orange-red microcrystalline solid (0.24 g, 62%). ^{1}H NMR (CD_3CN, all peaks appear as broad singlets): 50.2 (2H, *H*$_A$), 32.1 (2H, 2-Qn*H*), 26.2 (6H, N*Me*), 20.1 (2H, 3-Qn*H*), 16.2 (2H, *H*$_B$), 13.1 (2H, 6-Qn*H*), 13.0 (2H, 5-Qn*H*), 12.5 (2H, 7-Qn*H*), 2.23 (2H, 4-Qn*H*). MS (+FAB): *m*/*z* 564 [(M-(ClO$_4$)(CH$_3$))$^+$], 550 [(M − (ClO$_4$)(CH$_3$))$^+$], 497 [(M − (ClO$_4$)(CH$_3$CN)$_2$)$^+$]. Anal. Calcd. (found) for $C_{24}H_{22}F_6FeN_4O_6S_2$: C, 45.97 (45.92); H, 4.15 (4.03); N, 12.37 (12.28).

Crystallographic Details. Table 7 provides a summary of the crystallographic data for complexes [Fe(**1**)(OTf)$_2$], [Fe(**4**)(OTf)$_2$], and [Fe(**5**)(OTf)$_2$]. The structure of [Fe(**1**)(OTf)$_2$] was shown to be a partial racemic twin by a combination of *R*-factor tests [R_1^+ = 0.0402, R_1^- = 0.0477] and by the use of the Flack parameter [x^+ = +0.273(10), x^- = +0.727(10)]; the refinements using the Flack parameter gave the lower residuals quoted in Table 1 (CCDC 298281−298283).

VT Magnetic Susceptibility Measurements Via Evans' NMR Method. Magnetic susceptibilites in CD_2Cl_2 and CD_3CN solutions at 298 K were determined by Evans' NMR method.[58−61] Variable temperature magnetic moment determinations in an acetonitrile solution were carried out according to the methods described previously,[32,34] by using either a Bruker 400 MHz or a Bruker 500 MHz spectrometer and a 5 mm Wilmad Coaxial Insert NMR tube. Corrections for the change in solvent density with temperature were applied according to the data provided for CH_3CN,[62] and an additional factor (0.844/0.786) for the difference between the densities of CD_3CN (δ = 0.844 g/mL at 298 K) and CH_3CN (δ = 0.786 g/mL at 298 K) was applied. The concentration of the sample solutions was kept under 15 mM. Diamagnetic corrections were found to be insignificant and were therefore not applied. Thermodynamic parameters were determined according to the method described by Crawford and Swanson (see Supporting Information for more details).[33]

Standard Testing Conditions for the Oxidation of Cyclohexane. All catalytic oxidations were run at RT. The reaction products were analyzed by GC analysis, using GC-MS for product identification. All catalytic data quoted is the average of at least two runs. A 2.1 mmol (0.23 mL) portion of cyclohexane was added to a 75 × 25 mm sample vial containing 2.1 μmol of complex dissolved in 2.7 mL of acetonitrile and a small egg-shaped stirrer bar, and the mixture was stirred until the substrate had fully dissolved. A 0.3 mL portion of a 70 mM solution of hydrogen peroxide in acetonitrile was added dropwise over the course of 25 min to the stirred solution, by using a syringe pump. Upon completion of the

(58) Evans, D. F. *J. Chem. Soc.* **1959**, *36*, 2003−2005.
(59) Evans, D. F.; Fazakerley, G. V.; Phillips, R. F. *J. Chem. Soc.* **1971**, *24A*, 1931−1934.
(60) Evans, D. F.; Jakubovic, D. A. *J. Chem. Soc. Dalton Trans.* **1988**, 2927−2933.
(61) Grant, D. H. *J. Chem. Educ.* **1995**, *72*, 39−40.
(62) Kratze, H.; Müller, S. *J. Chem. Thermodyn.* **1985**, *17*, 151.

addition, the solution was stirred for an additional 15 min and was subsequently filtered through a pad of silica to remove the catalyst. The silica was then washed with 3.0 mL of acetonitrile and the washings were combined with the filtered reaction mixture. The final concentration of the components in the reaction mixture was cyclohexane = 700 mM, H_2O_2 = 7 mM, and catalyst = 0.7 mM. This gave a substrate/oxidant/catalyst molar ratio of 1000:10:1.

The acetonitrile solutions of hydrogen peroxide were prepared from commercially available 35% aqueous hydrogen peroxide and reagent grade acetonitrile. The resulting acetonitrile solution was used without drying. The silica pads used for catalyst removal were prepared by inserting a glass wool plug into a Pasteur pipet, onto which an approximately 25 mm deep layer of silica was added.

Acknowledgment. We are grateful to EPSRC and BP Chemicals Ltd. for a CASE award to J.E. Mr. Richard Sheppard and Mr. Peter Haycock are thanked for their assistance in NMR measurements.

Supporting Information Available: A crystalographic information file is provided for selected compounds. Diagrams and NMR data of compounds referenced herein are additionally included. A table of selected bond lengths and angles is also provided. This material is available free of charge via the Internet at http://pubs.acs.org.

IC070062R